Cobalt on dealuminated-Siβ as a catalyst for the oxidative dehydrogenation of propane

Stanislaw Dzwigaj, Diane Reja, Saremblé Koné-Guira, Antoine Miche, Guylène Costentin, Cyril Thomas

Cobalt on Dealuminated-Siβ as a Catalyst for the Oxidative Dehydrogenation of Propane

Stanislaw Dzwigaj, Diane Reja, Saremblé Koné-Guira, Antoine Miche, Guylène Costentin and Cyril Thomas*

Sorbonne Université, CNRS, Laboratoire Réactivité de Surface, LRS, F-75005 Paris, France.

* To whom correspondence should be addressed:

Dr. Cyril Thomas

Sorbonne Université, CNRS, Laboratoire Réactivité de Surface, LRS, UMR CNRS 7197, 4 Place Jussieu, Tour 43-53, 3ème étage, Case 178, F-75252, Paris, France

e-mail: cyril.thomas@sorbonne-universite.fr

Tel: + 33 1 44 27 36 30

Fax: + 33 1 44 27 60 33

ORCID:

Stanislaw Dzwigaj: orcid.org/0000-0003-1363-9316,

Antoine Miche: orcid.org/0000-0002-8006-1123,

Guylène Costentin: orcid.org/0000-0003-1559-6890,

Cyril Thomas: orcid.org/ 0000-0003-4224-6095

Graphical Abstract:

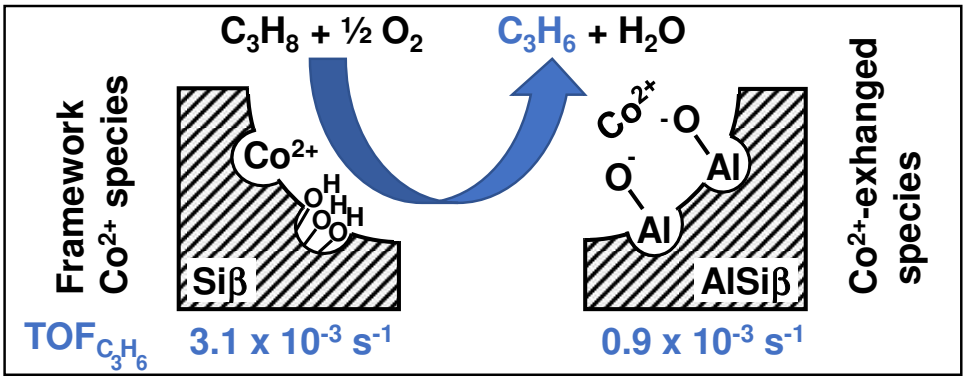

Highlights:

- $TOF_{C_3H_6}$ of Co^{2+} into Siβ is ~ 4 times higher than that of Co^{2+}-exchanged species
- $TOF_{C_3H_6}$ at 400 °C of Co-Siβ is ~ 7 times greater than that of V-Siβ
- Maximum incorporable content of Co as Co-Siβ is dictated by the amount of removable Al

Abstract:

The present work aims at investigating the oxidative dehydrogenation of propane (ODHP) catalytic properties of Co species supported on a Siβ zeolitic support. The Co^{2+} species incorporated in the silanol nests created by dealumination of a HAlSiβ pristine support (Co-Siβ) appeared to be about 4 times more active (3.1 x 10^{-3} s^{-1}) compared with that in exchange position of HAlSiβ (0.9 x 10^{-3} s^{-1}) for the formation of propene at 400 °C. The turn over frequency of the Co-Siβ samples are found to be greater than or equal to those reported in most of the earlier studies performed with Co-containing materials to date and to be about 7 times greater than that of V-Siβ materials (0.4 x 10^{-3} s^{-1}) from an earlier study, which illustrates the superiority of Co-Siβ over V-Siβ for the ODHP reaction. Maximum incorporable content of Co as Co-Siβ is dictated by the amount of removable Al.

Keywords: Catalysis, ODHP, propene, NO-TPD, XPS, Co-Siβ

1. Introduction

Propene (C_3H_6) is known as an essential platform chemical molecule for the production of polypropylene (60 %), acrylonitrile (9 %), oxo alcohol (8 %), propylene oxide (7 %) , cumene (6 %) and acrylic acid (4 %) [1]. The industrial production of propene is essentially achieved by steam reforming and fluid catalytic cracking of oil fractions [2-5]. The production of propene via the latter processes does not meet the market demand, however, which is known as the so-called propylene gap [5, 6]. The shale gas resources, comprising substantial amounts of ethane and propane, and the propylene gap renewed the interest in the valorization of propane to propylene. To meet the ever-increasing propene demand, about 110 million metric tons in 2018 [3, 7], the propane direct dehydrogenation (PDH) process has been industrialized [8]. Such a process obviously produces propene with the highest selectivity [7] and needs to be operated at relatively high temperatures, however, due the endothermicity of the dehydrogenation reaction [9], which makes it relatively energy intensive [8]. Another major drawback of the PDH process is related to the deactivation of the catalysts at such elevated temperatures with the deposition of carbonaceous species [8], which remediation requires periodic calcination of these deposits at high temperatures before a reduction step to regenerate the PtSn alloys [10].

Alternative processes are therefore sought for the production of propene in a more sustainable way, such as that of the oxidative dehydrogenation of propane (ODHP) [1-4]. This non-thermodynamically restricted exothermic process is favorably operated at lower temperatures and should be less sensitive to coke deposition because of the presence of oxygen in the reacting feed compared with the PDH process [1-4]. One major drawback of ODHP lies in the lower selectivity in propene compared to PDH due to overoxidation of propane and/or propene by oxygen by side reactions, which severely limits the industrial application of ODHP [2, 8].

Many efforts have been devoted to the study of ODHP catalysts for which metal-oxide based materials have been reported to be most active [4] before boron-containing materials showed promising properties rather recently [11, 12]. Over metal-oxide catalysts, ODHP has been shown to proceed via a Mars and van Krevelen mechanism [13] in which lattice oxygen species of the catalyst is involved in the oxidation process of the propane molecule, with the oxygen vacancies created by water release being replenished by molecular oxygen. The nature of the reacting oxygen species has been suggested to be of prime importance in this reaction for the selectivity in propene. The nucleophilic oxygen species were thus suggested to be much more selective for partial oxidation of propane compared with the electrophilic counterparts that lead to undesired combustion of propane/propene to CO_x ($CO + CO_2$) [3, 4, 14]. For metal-oxide based catalysts, those including vanadium [15, 16] have been shown to be among the most active in the ODHP reaction [14]. The nature of the supporting oxide [1] and the dispersion of V [3] have been shown to exhibit a drastic influence on the ODHP catalytic performance. Not only the nature of environment of the transition metal is important for ODHP but also the nature of the transition metal in itself. Several studies have reported on the promising properties of Co catalysts for the ODHP reaction indeed [17-30].

Following the pioneering works of Saxton et al. [31], Kim et al. [32] and Kraushaar and Van Hooff [33], Dzwigaj et al. [34] have shown that incorporation of V could be done in the silanol nests [35] created by dealumination of an HAlSiβ pristine support. Later, it was shown that such V-Siβ catalysts exhibited similar ODHP performance as that reported for vanadium supported on various SiO_2 supports [36]. Cobalt could also be inserted successfully in the silanol nests by Dzwigaj and co-workers [37-40] to be applied in NO selective catalytic reduction by ethanol [41] and ammonia [42-44], N_2O decomposition [42], dehydrochlorination [45] and Fischer-Tropsch

synthesis [46, 47]. As far as we know, the performance of Co-Siβ samples has not been reported in the ODHP reaction. The present work therefore aims at investigating the catalytic properties of Co species located in various environments of a β zeolitic support and to compare the performance of such species with earlier literature data reported on Co-based catalysts. In particular, the influence of the pH of the impregnating aqueous solutions was studied on the incorporation of Co^{2+} species in Siβ.

2. Experimental

2.1. Catalyst preparation

The synthesis of the Co_x-Siβ series of samples, which is schematically described in ref. [40], was done via a slightly modified two-step post-synthesis method developed earlier for the preparation of V-Siβ materials [34, 48].

2.1.1. Preparation of the HAlSiβ and Siβ supports

Briefly, the tetraethyl-ammonium β pristine zeolite (TEAβ, SINOPEC-RIPP, China, Si/Al ~ 14) was firstly calcined in a muffle furnace at 550 °C for 15 h to remove the TEA template and to produce the protonic form of the zeolite material (HAlSiβ). HAlSiβ (12 g) was then dealuminated in a nitric-acid solution (1 040 mL of concentrated HNO_3 (Aldrich, 68 wt% HNO_3) with 160 mL of distilled water resulting in a nitric acid concentration of 13 mol/L) at 80 °C for 4 h. The suspension was then cooled to RT and the solid was filtered before being washed with distilled water. Finally, the dealuminated material (Siβ, Si/Al ~ 400) was dried at 80 °C overnight in a laboratory oven.

2.1.2. Deposition of Co on Siβ

Deposition of Co was carried out by contacting 2 g of Siβ with 200 mL of $Co(NO_3)_2$ (Aldrich) aqueous solutions (from about 1.6 to 17.4 x 10^{-3} mol Co/L), either at pH 2.5 or 9.0, for 24 h under continuous stirring. The pH of these solutions was adjusted by adding drops of either concentrated nitric acid or ammonia solutions (Aldrich). Such a procedure led to Co loadings ranging from about 1 to 9 wt%. It must be stressed that the addition of the Siβ support in the $Co(NO_3)_2$ aqueous solutions at pH 9.0 resulted in a rapid decrease in the pH of the suspensions to about pH 3.0. In that case, the pH of the suspensions was then adjusted to pH 9.0 by addition of concentrated ammonia. The suspensions were then transferred in a rotary evaporator and water was evaporated under vacuum at 70 °C for about 2 h. As the ODHP reaction was performed up to 500 °C (Section 2.3.), the samples were calcined in a muffle furnace at 500 °C (100 °C/h) for 3 h. These series of samples will be referred to as Co_x-Siβ-pH-2.5 and Co_x-Siβ-pH-9.0, respectively, where *x* represents the Co loading (wt%).

2.1.3. Deposition of Co on HAlSiβ

For comparison, a sample including about 1.8 wt% Co was also prepared by wet impregnation of the HAlSiβ support ($Co_{1.8}$-HAlSiβ) by an aqueous solution of $Co(NO_3)_2$ following the same procedure as that described for the two previous series of samples but at pH 3.0.

2.2. Catalyst characterization

ICP-OES, XPS and H_2-TPR investigations were performed on the samples submitted to NO-TPD non-destructive experiments.

The chemical composition of the samples was ascertained by ICP-OES (Inductively Coupled Plasma Optical Emission Spectroscopy) using a 5100 SVDV spectrometer (Agilent) at the Plateforme ALIPP6 Laboratoire d'Analyse Géochimie Elémentaire (Sorbonne Université). The samples (50 mg) were firstly digested in a mixture of 1 mL of concentrated HF (Normatom, 47 wt%) and 1 mL of concentrated HNO_3 (68 wt%) at 80 °C for 2 h. Excess HF was then "neutralized" by 50 mL of an aqueous solution of H_3BO_3 (20 g/L) by complexation of the fluorides. The obtained solution was finally diluted with a diluted HNO_3 aqueous solution if necessary. Appropriate calibration mixtures were also used.

XP spectra were collected on an Omicron Scienta (Argus) X-ray photoelectron spectrometer using a monochromated Al Kα (hν = 1486.6 eV) radiation source having a 280 W electron beam power. Charge compensation was carried out using an electron beam having an energy of 1 eV and an emission current of 5 μA. The emission of photoelectrons from the sample was analyzed at a takeoff angle of 45° under ultrahigh vacuum conditions (1×10^{-7} Pa). XP spectra were collected at a pass energy of 20 eV for C 1s, O 1s, Si 2p, Al 2p and Co 2p core XPS levels. After data collection, because of the known difficulties in referencing the binding energies (BEs) to the C 1s line [49], the BEs were calibrated with respect to the BE of the Si 2p peak (FWHM ~ 1.8 eV) at 103.3 eV [44, 50, 51]. All of the BEs reported in this work were measured within an accuracy of ±0.2 eV. The peak areas were determined after subtraction of a Tougaard background. The atomic ratio calculations were performed after normalization using Scofield factors [52]. Spectrum processing was carried out using the Casa XPS software package and Origin 7.1 (Origin Lab Corporation). The $Co_{3.0}$Siβ-pH-2.5 and $Co_{3.1}$Siβ-pH-9.0 samples were also analyzed by XPS after ODHP reaction.

Temperature-Programmed Reduction by hydrogen (H_2-TPR) experiments were performed by using a Micromeretics 2920 equipment. 40 to 50 mg of the sample was introduced in the U-type reactor on a plug of quartz wool and submitted to oxidation under 25 mL/min O_2(5%)/He from RT to 500 °C (10 °C/min) and maintained at 500 °C for 1 h. It was found that the samples did not exhibit any oxidation contribution (**Figure S1**), indicating that previous NO-TPD experiments did not lead to the reduction of the Co species. The samples were then cooled to RT under the O_2(5%)/He flow. After purging by Ar (25 mL/min), the samples were submitted to H_2-TPR under 25 mL/min H_2(5%)/He from RT to 900 °C (10 °C/min) and left at this temperature for 2 h. Water release in H_2-TPR experiments was trapped with an isopropanol-liquid N_2 mixture prior to the TCD detector.

NO Temperature-Programmed Desorption (NO-TPD) experiments were carried out in a U-shape quartz reactor (10 mm i.d.). The samples (about 0.12 g) were held on a plug of quartz wool and the temperature was controlled by a Eurotherm 2408 temperature controller using a K-type thermocouple. Reactant gases (Air Liquide) were used as received and fed from independent gas cylinders by means of mass flow controllers (Brooks 5850TR) with a total flow rate of 230 mL_{NTP}/min. The reactor outlet was continuously monitored by chemiluminescence NO_x analyzers (Thermo Environmental Instruments 42C-HL or Eco Physics CLD 700 AL) that allowed the simultaneous detection of NO and NO_2 (NO_x = NO + NO_2). Prior to the NO-TPD experiments, the samples were annealed in situ in He or Ar at 500 °C (3 °C/min) for 2 h under a flow rate of 100 mL_{NTP}/min. Following the in-situ annealing treatment, the samples were exposed to the adsorption mixture that consisted of 400 ppm NO diluted in He or Ar. The samples were exposed to the adsorption mixture at RT for about 2 h until the outlet NO_x readout was equivalent to the inlet NO_x readout. The latter parameter was set to ensure that each sample was saturated under the present experimental conditions. Before the NO-TPD step, the samples were flushed in He or Ar at RT for

about 1 h to remove weakly chemisorbed species until the NO and NO_2 concentrations detected at the outlet of the reactor were found to be negligible. NO-TPD experiments were carried out from RT to about 500 °C at a heating rate of 3 °C/min under a flow of 230 mL_{NTP}/min of He or Ar. It was checked on two aliquots of $Co_{1.0}$Siβ-pH-2.5 that both NO_x analyzers provided similar NO_x-TPD profiles (**Figure 1**) and NO_x uptakes (105 and 102 µmol/g). It must be noted that only traces of NO_2 were detected over the Co_x-Siβ-pH-2.5 and Co_x-Siβ-pH-9.0 series, whereas significant quantities of NO_2 were recorded over HAlSiβ and $Co_{1.8}$-HAlSiβ, the origin of which may be attributed to NO disproportionation ($3\ NO = N_2O + NO_2$) [53].

2.3. ODHP catalytic experiments

Prior to the catalytic runs, the Co_x-Siβ-pH-2.5, Co_x-Siβ-pH-9.0 and $Co_{1.8}$-HAlSiβ samples (~ 20 µmol of Co) diluted in 0.6 g of α-Al_2O_3 (125-200 µm, Aldrich) were calcined in O_2 (2.2%)–He (65.1 mL_{NTP}/min) at 500 °C (2 °C/min) for 3 h unless specified otherwise. The temperature was then decreased to 400 °C. The ODHP experiments were carried out in a U-type quartz reactor (10 mm i.d.). The samples were held on a plug of quartz wool, and the temperature was controlled by a Eurotherm 2408 temperature controller using a K type thermocouple. Reactant gases (Air Liquide, used as received) were fed from independent mass flow controllers (Brooks 5850TR and Bronkhorst F-201CV-200-RAD-11-V). Typically, the composition of the C_3H_8-O_2-He (4.3–1.0–47.3) reaction mixture was: 8.2 % C_3H_8 and 1.9 % O_2 in He with a total gas flow of 74.1 mL_{NTP}/min. The catalyst was contacted with the reaction mixture at 400 °C and the temperature was increased by steps of 25 °C (5 °C/min) up to 500 °C for about 1 h 30 at each reaction step at atmospheric pressure. After reaction at 500 °C for 1 h 30, the catalyst was cooled to 400 °C under the reaction mixture. Analysis of the composition of the reactor outflow was performed on-line with a µ-GC

(Varian, CP4900) using three different columns running in parallel. The 5A molecular sieve column (80 ºC, 150 kPa He, 200 ms injection time, 30 s backflush time) was used to separate H_2, O_2, CH_4 and CO. The poraplot Q column (100 °C, 150 kPa He, 50 ms injection time, 6 s backflush time), was used to separate CO_2, C_2H_4, C_2H_6, H_2O, C_3H_6 and C_3H_8. The CP-SIL5 column (45 °C, 150 kPa He, 50 ms injection time) was used to separate C_3H_6O compounds (acetone + propenal) from C_3H_4O (acrolein).

The conversion of C_3H_8 (X C_3H_8) and the product selectivities (S A_i) were calculated as follows:

$$X\ C_3H_8\ (\%) = (\Sigma n_i\ [A_i] / (3 \times [C_3H_8]_{inlet})) \times 100$$

$$S\ A_i\ (\%) = (n_i\ [A_i] / \Sigma n_i\ [A_i]) \times 100$$

where n_i, $[A_i]$ and $[C_3H_8]_{inlet}$ are the number of carbon atoms in the A_i products, the concentrations of the A_i products, and the inlet concentration of propane, respectively.

For comparison with earlier literature data, the formation of C_3H_6 in the ODHP catalytic reaction was calculated as turnover frequencies (TOFs) [54] normalized by the total number of Co atoms such as:

$$TOF\ (s^{-1}) = (([C_3H_6] \times F) / (100 \times V_m)) / (sw \times \%Co) / (100 \times M_{Cobalt})),$$

Where $[C_3H_6]$, F, V_m, sw, %Co and M_{Cobalt} are the concentration in C_3H_6 at the outlet of the reactor (%), the total flow rate (mL s^{-1}) at 0 °C and 101 325 Pa, the molar volume (22414 mL mol^{-1}) at 0 °C and 101 325 Pa, the sample weight (g), the Co content (wt%) and the atomic weight of Co (58.933 g mol^{-1}), respectively.

Under the present experimental conditions, it was checked that the reactor loaded with 0.6 g of α-Al_2O_3 did not contribute to the transformation of C_3H_8 to a significant extent at 400 °C (**Figure S2**)

and that both C_3H_8 and O_2 conversions measured at 400 °C varied proportionally to the amount of sample loaded in the reactor, indicating the absence of external limitations. The carbon and oxygen balances were found to be above 98 and 90 %, respectively.

3. Results and discussion

3.1. Speciation of Co in the impregnating solutions

The speciation of Co in the aqueous medium was computed [55] as a function of the pH of the aqueous medium (by addition of HNO_3 or NH_3) for the lowest (**Figure 2**a) and the greatest (**Figure 2**b) Co concentrations used for the preparation of the materials. As illustrated in **Figure 2**a, Co remains as $Co(H_2O)_6^{2+}$ species up to pH 8.0. At higher pH, the precipitation of $Co(OH)_2$ occurs in agreement with an earlier literature report [56]. $Co(OH)_2$ appears to be the dominant species up to about pH 11 before the appearance of various Co amine complexes at higher pH. A comparable trend is observed for the highest Co concentration (**Figure 2**b) with a shift of the $Co(OH)_2$ precipitation frontier to lower pH, however. Overall, it can be deduced from **Figure 2** that Co should be essentially present as $Co(H_2O)_6^{2+}$ at pH 2.5, whereas it should precipitate to $Co(OH)_2$ at pH 9.0 for all of the Co concentrations used in the present work for the preparation of the materials.

3.2. Characterization of the samples

XRD, ^{1}H, ^{27}Al and ^{29}Si MAS NMR, FTIR and DR-UV-vis complementary data recorded on selected samples can be found in an another article [40]. Briefly, it was found that dealumination of the HAlSiβ pristine support led to a contraction of the zeolite structure (XRD), a significant

decrease in the intensity of the ^{27}Al NMR signals and an increase in that of the ^{1}H NMR signals, and an increase in the intensity of the OH IR contributions in agreement with earlier studies [34, 36-47]. These data corroborated the extraction of the framework Al species under strongly acidic conditions and the corresponding formation of silanol nests in the dealuminated Siβ support. The addition of Co to the dealuminated Siβ support led to an expansion of the zeolite structure (XRD) [37-47] and a pronounced decrease in the intensity of the ^{1}H NMR signals [47] and the OH IR contributions [37-40, 42, 47], attesting for the incorporation of Co^{2+} ions into the Siβ framework and the formation of various Co species as indicated by DR-UV-vis spectroscopy [37, 40-44, 57].

3.2.1. Chemical composition ascertained by ICP-OES

The chemical composition of the samples deduced from ICP-OES analyses (**Table 1**) shows that the amount of Co deposited agrees reasonably with that targeted. The Si/Al ratio of the pristine support HAlSiβ was found to be about 14 in agreement with the expected value (Section 2.1.), whereas those of the dealuminated Siβ and Co_x-Siβ samples increased to 380 and 500 ± 40, respectively. The lower Si/Al ratio of the Siβ support (380) compared to those of the Co_x-Siβ materials (500 ± 40) may be attributed to further dealumination of the Siβ support in the course of the deposition step of Co that was performed at low and high pH for 24 h (Section 2.1.). Dealumination of the pristine HAlSiβ support has been reported to result in the creation of silanol nests in the Siβ structure [34, 36-39].

3.2.2. XPS

The binding energies (BEs) of the O 1s, C 1s, Al 2p and Co $2p_{3/2}$ core levels of the samples are summarized in **Table 2**. The narrow peak (FWHM ~ 1.7 eV) of the O 1s core level with a fairly

constant BE (~ 532.5 eV) can be attributed to O^{2-} species from the Siβ crystalline network [51, 58, 59].

The presence of adventitious carbon was also detected on all samples at 283.8-284.9 eV (13 ± 1 at. %). The fact that the BE of C 1s core level varied by about 1 eV may be attributed to imperfect compensation of the local charging of the non-conductive materials despite the use of a flood gun, which provides support for using the Si 2p (**Figure S3**) as a reference rather than adventitious carbon [49].

Al 2p peaks (74.5 eV, FWHM ~ 2.2 eV) attributed to Al^{3+} species [51, 59] could only be observed on the non-dealuminated HAlSiβ and $Co_{1.8}$-HAlSiβ samples in agreement with other XPS measurements [40]. The surface Si/Al at. ratio of the non-dealuminated samples (**Table 2**) was found to be in good agreement with the bulk Si/Al ratio determined by ICP-OES (**Table 1**), indicating that Al was homogeneously distributed in the HAlSiβ pristine material. Given that residual amounts of Al could be measured by ICP-OES on the dealuminated Siβ samples (**Table 1**), the absence of Al 2p signal on these samples may be assigned to the presence of residual Al atoms in the core of the dealuminated Siβ grains whose Al 2p core level signal would be screened by the silicon atoms of the outer layers. This suggests that dealumination of the pristine HAlSiβ support was easier to achieve on the outer layers of the zeolite grains rather than in their cores. The presence of residual Al found by ICP-OES in the dealuminated Siβ samples appears to be consistent with the presence of an ^{27}Al MAS NMR peak at 51-54 ppm [40, 47] characteristic of tetrahedrally coordinated Al^{3+} species in the Siβ zeolite framework.

The Co 2p core level showed essentially the characteristic spin-orbit doublet (Co $2p_{1/2}$ at ca. 797 eV and Co $2p_{3/2}$ at ca. 781 eV, **Table 2**) with shake-up satellites at about 803 and 786 eV (**Figure S3**), indicating the presence of Co^{2+} species in the prepared samples. Whereas the BE of

the Co $2p_{3/2}$ signal remained essentially constant and close to 781.3 eV on the Co_x-Siβ series prepared at pH 2.5 and 9.0 (**Table 2**), it is of interest to notice that the BE of the Co $2p_{3/2}$ signal of $Co_{1.8}$-HAlSiβ appeared to be recorded at a substantially higher BE (782.5 eV, **Table 2**). In agreement with the earlier study of Boix and Fierro, performed over various zeolitic matrixes [60], such an elevated BE is consistent with the presence of Co^{2+} species acting as charge compensation cations on the non-dealuminated pristine support. The Co $2p_{3/2}$/Si 2p surface at. ratios are plotted as a function of the bulk Co/Si at. ratios deduced from ICP-OES in **Figure 3**. This figure firstly shows that the Co $2p_{3/2}$/Si 2p surface at. ratios are much smaller than the bulk ones over all of the investigated samples in line with an earlier study [44]. Such a discrepancy may be accounted for by a screening effect of the Co signal by the Si atoms from the β zeolite network. In addition, it can be seen that the Co $2p_{3/2}$/Si 2p surface at. ratio varies reasonably linearly with respect to the bulk one over the whole range of compositions of the investigated samples, which indicates that the dispersion state of the Co atoms remained essentially comparable over the various series of samples from an XPS viewpoint.

3.2.3. H_2-TPR

The H_2-TPR profiles on both series of samples are shown in **Figure 4**. The Co_x-Siβ-pH-2.5 samples showed essentially a reduction peak at high temperature at about 800 °C (**Figure 4**a). A shoulder also appeared at about 730 °C for $Co_{5.6}$-Siβ-pH-2.5 (arrow in **Figure 4**a) and the reduction of the samples including a Co loading greater than or equal to 1.9 wt% was found to begin at lower temperature (~ 700 °C) compared to that of $Co_{1.1}$-Siβ-pH-2.5 (~ 770 °C, **Figure 4**a). The Co_x-Siβ-pH-9.0 samples showed a reduction peak at about 800 °C as well (**Figure 4**b). For the most highly loaded samples (Co content greater than or equal to 4.3 wt%), a reduction peak is also observed at

about 330 °C. As also reported in [40], the $Co_{1.8}$-HAlSiβ sample did not exhibit any H_2 reduction feature (**Figure S4**), indicating that the Co^{2+} species on charge compensation sites did not reduce below 900 °C [45, 61-63]. On the Co_x-Siβ series, the high-temperature peak can therefore be assigned to the reduction of framework pseudo-tetrahedral Co(II) species in strong interaction with the Siβ support [37-42], whereas that at about 330 °C can be assigned to the reduction of Co_3O_4 crystallites. Yet these Co_3O_4 crystallites could not be detected by XRD on $Co_{4.3}$Siβ-pH-9 [40] likely because of being too small and/or in low amount [61]. The consumption of H_2 in the H_2-TPR experiments amounted to be about 72 ± 21 % of the Co content (**Figure 4**), as already reported earlier on similar samples [42]. At the lower contents of Co, the high-temperature reduction peak appears to be incomplete, in other words the signal does not return to baseline, and this may be at the origin of an underestimation of the amount of Co reduced in the H_2-TPR experiments.

3.2.4. NO_x-TPD

Earlier studies have reported on the interaction of NO with Co^{2+} species on various zeolitic materials and the use of temperature-programmed desorption experiments as a tool to characterize these materials [43, 64-66]. Under the present experimental conditions, it was found that the dealuminated support (Siβ) did not chemisorb NO (**Figure S5**) in agreement with previous studies performed on various silica materials [67-69]. In contrast, the HAlSiβ pristine carrier exhibited two desorption peaks at 100 and 320 °C (**Figure 5**a) in agreement with the earlier work of Dzwigaj and co-workers [43]. The greater NO uptake of HAlSiβ (65 µmol/g), determined from the profile shown in **Figure 5**a (purple trace), compared to that reported previously (8 µmol/g, [43]) can be attributed to differences in adsorption temperatures [66]. The marked difference in NO uptake between Siβ and HAlSiβ demonstrates that the presence of Al is instrumental in the chemisorption of NO on a

Co-free sample and makes more complicated the estimation of the NO uptake by the Co^{2+} species, and the corresponding NO/Co ratio, for $Co_{1.8}$HAlSiβ. **Figure 5**a shows that the addition of Co to HAlSiβ leads to a significant increase in the amount of NO desorbed (195 μmol/g, gray trace) compared to that of the pristine HAlSiβ support (65 μmol/g, purple trace). This indicates that NO also interacted with the Co^{2+} exchanged species of $Co_{1.8}$-HAlSiβ to a significant extent. The chemical composition of $Co_{1.8}$-HAlSiβ (**Table 1**) indicates that about 63 % of the protons have been exchanged by the Co^{2+} species (Co/Al ~ 0.31) on such sample. Considering this together with (i) the amount of NO desorbed from this sample (195 μmol/g) and that from the pristine HAlSiβ support (65 μmol/g) and (ii) assuming that Co^{2+}-charge-compensated AlO^- sites did no longer contribute to NO desorption from the HAlSiβ support, the NO/Co molar ratio can be estimated to be about 0.56 for $Co_{1.8}$-HAlSiβ.

Finally, the NO-TPD profile recorded on $Co_{1.8}$-HAlSiβ (**Figure 5**a, grey trace) does not resemble any of the TPD profiles described in earlier studies [64-66, 70]. This may be attributed to differences in the TPD experimental conditions and/or to the nature of the studied samples. In addition, small amounts of NO_2 were also observed in the course of the NO-TPD experiments performed on HAlSiβ and $Co_{1.8}$-HAlSiβ at 130 and 220 °C, respectively. The formation of NO_2 may be due to NO disproportionation ($3\ NO = NO_2 + N_2O$), as suggested previously by Addison and Barrer on Na-zeolites [53].

Regarding the Co samples prepared with the dealuminated support (**Figure 5**b,c, Co_x-Siβ-pH-2.5 and Co_x-Siβ-pH-9.0 series), the desorbed species can be attributed exclusively to NO interacting with the Co^{2+} species, as it was found that the Siβ bare support did not chemisorb NO (**Figure S5**). The TPD profiles recorded on both series showed a main NO desorption peak at about

80 °C and two additional contributions of much weaker intensity at about 200 and 330 °C. On a comparable sample (Co(PS)SiBEA), Dzwigaj and co-workers [43] reported only one NO desorption peak at 190 °C, which is not inconsistent with the NO-TPD profiles reported in the present work. Firstly, it must be highlighted that the adsorption step on Co(PS)SiBEA was carried out at 70 °C [43], thus at a temperature close to that for which the main desorption peak was observed in the present study (**Figure 5**b,c), which would explain the absence of such contribution in the work of Dzwigaj and co-workers [43]. Secondly, the contribution of weak intensity observed at 200 °C (**Figure 5**b,c) is consistent with that observed earlier at 190 °C by Dzwigaj and co-workers [43]. Thirdly, given that the contribution at 330 °C is generally of weaker intensity than that at 200 °C (**Figure 5**b,c), such a contribution may have remained below detection limits in the work of Dzwigaj and co-workers [43]. Definitive assignment of the observed NO contributions (**Figure 5**b,c) remains uncertain. Earlier studies performed on similar Co-Siβ materials have shown essentially the formation of dinitrosyl complexes with NO adsorption followed by FTIR [38, 43]. In particular, Mihaylova et al. have reported that two different $Co^{2+}(NO)_2$ dinitrosyls were formed on Co-Siβ [38]. Over an exchanged Co-ZSM-5 material, Zhang et al. have showed that the decomposition temperatures of two Co dinitrosyl complexes was strongly dependent on the nature of the dinitrosyl complex [70]. The multiple NO peaks observed in the NO-TPD experiments (**Figure 5**b,c) may therefore be attributed to the decomposition of various dinitrosyls, and the potential decomposition of mononitrosyls [38] in the Co_x-Siβ materials. Additional work would obviously be needed to ascertain such assumptions.

The NO uptakes deduced from the NO-TPD profiles (**Figure 5**b,c) are displayed in **Figure 5**d. Overall, it can be seen that the NO uptakes are similar on both series of Co_x-Siβ of samples and therefore that the pH at which Co was deposited did not exhibit a significant influence on the

dispersion of the Co species for comparable Co loadings. The NO/Co ratios estimated from the amounts of NO desorbed are plotted in **Figure 5**e. The NO/Co ratios of the most lowly loaded samples of both series ($Co_{1.1}$-Siβ-pH-2.5: NO/Co = 0.56 and $Co_{0.9}$-Siβ-pH-9.0: NO/Co = 0.43), for which the highest dispersion of the Co^{2+} species may be assumed, are found to be comparable to that found for Co^{2+} cations on exchanged position of $Co_{1.8}$-HAlSiβ (NO/Co = 0.56). This suggests that the NO adsorption properties of the Co^{2+} species supported on the dealuminated Siβ support should not be affected to a significant extent compared to those of the Co^{2+} cations in exchanged position present in $Co_{1.8}$-HAlSiβ. The fact that the NO/Co ratios are found to be much lower than that expected with the formation of dinitrosyls [38], which still remains unclear at the present stage, therefore prevents the use of the NO-TPD data for a quantitative determination of the Co dispersion on the samples. Yet these data can be used to compare the dispersion of Co in the studied materials from a qualitative viewpoint. Within each series of samples, namely Co_x-Siβ-pH-2.5 or Co_x-Siβ-pH-9.0, **Figure 5**e shows that the NO/Co ratio decreases as the Co content increases, as also reported by Gutierrez et al. [65] on various Co/mordenite materials. The decrease in NO/Co ratio (**Figure 5**e) can be attributed to a decrease in the dispersion of the Co species as the Co content increases with the formation of Co_xO_y species [65]. Overall, the NO uptakes obtained in the present study are found to be lower than those reported on Co-zeolite materials in previous studies [64-66, 70]. This probably relies both on differences in the studied materials and the experimental conditions under which the NO-TPD experiments were performed. In these earlier studies, the NO-TPD experiments have been carried out on various zeolite supports such as ZSM5 [64, 70], Y [64, 66, 70], Mordenite [64, 65, 70] and β [66]. Li and Armor have reported that the nature of the zeolite support was decisive for the chemisorption of NO when exchanged by Co^{2+} ions [64]. In addition, part of the NO uptakes has been recorded on H-zeolite supports [64-66], whereas it was shown in

the present study that the presence of protons in the zeolite support increased the NO uptake to a significant extent (**Figure 5**a). Finally, the NO partial pressures used in these earlier studies were much higher (1000 – 2000 ppm NO) than that used in the present study (400 ppm), and this parameter has been suggested to influence the NO/Co stoichiometry [64].

Overall, the characterization of the Co_x-Siβ series of samples performed by H_2-TPR (Section 3.2.3.) and NO-TPD (Section 3.2.4.) seems to indicate that Co(II) species (XPS, Section 3.2.2.) may be involved in various environments depending on the Co loading. Yet the quantification of the various Co species has been reported to be extremely challenging in the case of Co^{2+}-exchanged HAlSiβ materials [71].

3.3. ODHP catalytic results

Prior to evaluation of the Co samples, the thermal reaction between C_3H_8 and O_2 was probed in a reactor loaded with 600 mg of α-Al_2O_3 (**Figure S2**). C_3H_8 conversion, increasing from 0.1 to 1.0 % from 400 to 500 °C, was found to be mainly due to the complete oxidation of propane to carbon oxides (CO_x = CO + CO_2) with a selectivity of about 80 ± 3 % in the latter by-products. Traces of methane, ethane, ethylene, acetone/propenal and acroleine were observed above 450 °C, whereas detectable amounts of H_2 were recorded above 475 °C. The formation of C_3H_6 was also recorded and found to increase from 12 to about 220 ppm from 400 to 500 °C, resulting in a C_3H_6 selectivity of about 14 ± 2 %. As the thermally assisted formation of C_3H_6 was found to be limited at 400 °C, comparison of the catalytic performance of the various samples was made at such a temperature. Finally, the conversion of O_2 increased from 2 to 22 % as the reaction temperature increased from 400 to 500 °C.

Bian et al. have reported recently that highly dispersed tetrahedrally coordinated Co(II) species, stabilized on a mesoporous silica, efficiently catalyzed the direct dehydrogenation of C_3H_8 (PDH) at 600 °C [72]. Although PDH has been reported to remain thermodynamically disfavored below about 550 °C [56], Davis and co-workers [73], and Wang et al. [74] showed that such a reaction could be catalyzed at 500 and 550 °C by Co(II) single-sites supported on N-doped carbon and ordered SiO_2 channels, respectively. By removing O_2 from the ODHP reacting feed at 400 °C, it was verified that PDH did not contribute to the production of C_3H_6 to a significant extent under our conditions on $Co_{3.0}$-Siβ-pH-2.5 and $Co_{3.1}$-Siβ-pH-9.0 (**Figure S6**), however.

O_2, CO_x and C_3H_6 concentrations, and C_3H_8 conversion are displayed in **Figure 6** as a function of time on stream and reaction temperature for the catalysts loaded with about 2 wt % Co. As expected, C_3H_8 conversion, CO_x and C_3H_6 concentrations increased, whereas O_2 concentration decreased as the reaction temperature increased for all of the samples. **Figure 6** shows that the catalyst prepared from the HAlSiβ pristine support ($Co_{1.8}$-HAlSiβ, **Figure 6**c) appeared to be the least active sample among the samples containing about 2 wt % Co. By comparing the initial C_3H_8 conversion at 400 °C with that recorded at 400 °C after reaction at 500 °C, $Co_{1.9}$-Siβ-pH-2.5 (**Figure 6**a) and $Co_{1.8}$-HAlSiβ (**Figure 6**c) appeared to have suffered from deactivation after reaction at 500 °C by about 22 and 25 %, respectively (**Table 3**). Deactivation of theses samples could be observed from 400 to 475 °C and 475 to 500 °C for $Co_{1.9}$-Siβ-pH-2.5 (**Figure 6**a) and $Co_{1.8}$-HAlSiβ (**Figure 6**c), respectively. In contrast, $Co_{2.2}$-Siβ-pH-9.0 was found to be activated (**Figure 6**b) by about 13 % after reaction at 500 °C (**Table 3**). Except $Co_{1.1}$-Siβ-pH-2.5, which was found be stable, the other samples of the Co_x-Siβ-pH-2.5 series were found to deactivate after reaction at 500 °C (**Table 3**). C_3H_8 conversion at 400 °C after reaction at 500 °C was found to be close to 3 % with a selectivity in C_3H_6 of about 50 % for a Co content lower than or equal to

3.0 wt % in the Co_x-Siβ-pH-2.5 series. Above this Co loading, the conversion of C_3H_8 was found to decrease substantially and the selectivity in C_3H_6 was found to decrease at the highest Co loading (9.3 wt %) only. Similar trends were also observed for the Co_x-Siβ-pH-9.0 series (**Table 3**), except that C_3H_8 conversion and C_3H_6 selectivity appeared to remain essentially constant up to a higher Co loading (4.3 wt %) compared to the Co_x-Siβ-pH-2.5 series (3.0 wt %). It can be noticed that C_3H_6 selectivity increased substantially for catalysts exhibiting a deactivation greater than or equal to 16 % in the Co_x-Siβ series (**Table 3**). This increase in C_3H_6 selectivity cannot be attributed to a significant increase in the production of C_3H_6 (**Table 4**). A close inspection of the evolution of the CO_x concentration with time on stream for $Co_{1.9}$-Siβ-pH-2.5 (**Figure 6**a) shows that the increase in C_3H_6 selectivity from 36 to 47 % (**Table 3**) was mainly due to a significant decrease in the production of CO_x after reaction at 500 °C, as the concentration of C_3H_6 was found to remain essentially constant (**Figure 6**a, **Table 3**). The sintering of part of the Co species could be ruled out as the origin of the decrease in CO_x production after ODHP reaction at 500 °C since the XPS Co/Si at. ratios of $Co_{3.0}$Siβ-pH-2.5 (Co/Si = 0.0099) and $Co_{3.1}$Siβ-pH-9.0 (Co/Si = 0.0118) were found to remain essentially constant after ODHP reaction (0.0107 and 0.0122, respectively). It must also be noticed that increasing amounts of H_2, most probably produced via the water-gas shift reaction [75], were recorded with increasing temperatures on all of the samples investigated in the present study, as also reported in earlier studies ([2] and references therein). In the present study, the production of H_2 could be recorded even if complete conversion of O_2 was not always achieved. In contrast, the production of H_2 on V-Siβ catalysts may be attributed to the occurrence of the PDH reaction as H_2 could only be observed at temperatures for which full O_2 conversion was achieved [36]. More recently, some of us also recorded the production of H_2 in the ODHP reaction over V-modified hydroxyapatite catalysts at temperatures for which full conversion of O_2 was not achieved

[76]. In this latter study, the occurrence of the PDH reaction could be discarded since the removal of O_2 from the reacting feed led to almost complete disappearance of C_3H_6 in the effluent, as is also the case over the Co_x-Siβ materials prepared in the present study (**Figure S6**). The concentration of H_2 at 500 °C was found to be about 0.7 % for the Co_x-Siβ-pH-2.5 samples containing from 1.1 to 5.6 wt % of Co, whereas $Co_{9.3}$-Siβ-pH-2.5 produced 0.06 % of H_2 only. The amounts of H_2 produced on the Co_x-Siβ-pH-9.0 series were found to be slightly higher than those found on the Co_x-Siβ-pH-2.5 series, whereas that produced on $Co_{1.8}$-HAlSiβ was much lower (0.2 %). These data show that the samples were exposed to hydrogen at relatively high temperatures in the course of the ODHP reaction. The significant increase in C_3H_6 selectivity observed for samples exhibiting a deactivation greater than or equal to 16 % (**Table 3**), which is essentially attributed to a significant decrease in CO_x production after reaction at 500 °C (**Figure 6**a), may be attributed to changes in the oxidation state and/or coking of some Co species (probably present in small quantities) under the experimental conditions of the ODHP reaction, such as CoO_x species that have been reported to be fairly active in the oxidation of propane [77].

After reaction at 500 °C, the ODHP catalytic activity of $Co_{1.9}$-Siβ-pH-2.5 was recorded at 400, 375 and 350 °C before being measured once more at 400 °C (**Figure S7**). The fact that the catalytic activity recorded at 400 °C after measurements at 375 and 350 °C was found to be identical to that recorded at 400 °C after reaction at 500 °C indicates that the measurements were performed on a stabilized catalytic sample. The apparent activation energies for the production of C_3H_6 and CO_x were estimated to be about 87 and 108 kJ mol^{-1}, respectively, from the corresponding Arrhenius plots in the 350-400 °C temperature domain (**Figure S8**). The fact that the apparent activation energy for the production of C_3H_6 is consistent with earlier data for this reaction [36] suggests that the rate measurements were performed in a kinetic regime free of diffusion limitation.

The turnover frequencies (TOFs), normalized by the total number of Co atoms (Section 2.3.) and determined at 400 °C after reaction at 500 °C, are listed in **Table 5**. This table shows firstly that $Co_{1.8}$-HAlSiβ was the least active sample (0.86 x 10^{-3} s^{-1}) of the investigated catalysts. Moreover, it can be seen that the TOFs remained essentially constant and close to 3.07 ± 0.45 x 10^{-3} s^{-1} for samples with Co loadings below 5 wt % for both Co_x-Siβ series, and were found to decrease at Co loadings higher than 3.0 and 4.3 wt% in the Co_x-Siβ-pH-2.5 and Co_x-Siβ-pH-9.0 series, respectively. It must be highlighted that the TOF measured in the present work over Co (3.07 x 10^{-3} s^{-1}) is found to be about 7 times higher than that reported earlier for vanadium in comparable materials (0.44 x 10^{-3} s^{-1} [36]). The superiority of Co over V for ODHP is likely responsible for the interest in Co for this reaction [17-30]. The evolution of the TOF measured at 400 °C after ODHP reaction at 500 °C over the Co_x-Siβ series (TOF essentially constant below 5 wt% Co and decreasing at higher Co contents, **Table 5**) cannot be correlated straightforwardly with the Co speciation deduced from H_2-TPR (Section 3.2.3., **Figure 4**). This may be attributed to the fact that H_2-TPR profiles were recorded on samples in their calcined state, whereas TOFs were estimated at 400 °C after ODHP reaction at 500 °C, which may have affected the Co speciation in the spent catalysts compared to that in the calcined samples. This may also be attributed to the fact that only a limited number of Co species were active in the ODHP reaction, as reported earlier in propane-SCR [71]. More interesting is that the above-mentioned evolution of the TOF in the Co_x-Siβ samples can be correlated to the changes in C_3H_6 production observed at 400 °C before and after ODHP reaction at 500 °C (**Table 4**). **Table 4** shows a slight increase in C_3H_6 production after ODHP reaction at 500 °C for the Co_x-Siβ samples with a Co loading below 5 wt%, whereas a decrease in C_3H_6 production can be observed for Co loadings greater than 5 wt% indeed. The fact that the TOFs were found to remain essentially constant below 5 wt % of Co in the Co_x-Siβ series

may be attributed to the maximum content of Co incorporable in the silanol nests created by dealumination of the HAlSiβ pristine support. On a one-to-one $Co_{inserted}$-to-$Al_{extracted}$ basis, the decrease in Al content from 2.65 to 0.11 wt% after dealumination of the HAlSiβ support to Siβ (**Table 1**) would lead to a maximum Co loading of about 5.6 wt% indeed. Below the maximum content of Co incorporable in the silanol nests on both Co_x-Siβ series, it may appear surprising that the C_3H_6 TOF did not depend on the speciation of Co in the impregnating solutions (pH 2.5 and 9.0). **Figure 2** shows that Co speciation in the aqueous medium remained as $Co(H_2O)_6^{2+}$ at pH 2.5, whereas the precipitation of $Co(OH)_2$ was deduced to occur at pH 9.0, indeed. Such an unexpected result may be attributed to the transient decrease to pH 3.0 during the addition of the Siβ support to the Co solution at pH 9 (Section 2.1.). Under such acidic conditions, the $Co(OH)_2$ precipitate produced at pH 9.0 (**Figure 2**) may be dissolved rapidly to $Co(H_2O)_6^{2+}$, allowing for the incorporation of Co in the Siβ framework as is the case in the preparation of the Co_x-Siβ materials at pH 2.5. As the pH of the suspensions was subsequently adjusted back to pH 9.0 (Section 2.1.), the incorporation of Co in the framework of the Siβ support is assumed to be a rather rapid process, as reported for V incorporation in Siβ, which was shown to be kinetically promoted under acidic conditions [78].

Table 6 lists the C_3H_6 turnover frequencies (TOFs) on a per atom (Co or V) basis reported in earlier ODHP works at various temperatures. These earlier data are essentially compared to those estimated in the present study over the $Co_{1.9}$-Siβ-pH-2.5 sample, which was shown to be representative of the most active samples (**Table 5**). Firstly it can be noted that the TOF value at 400 °C reported by Bulánek et al. (0.75×10^{-3} s^{-1}, **Table 6** [19]) compares remarkably well with that obtained for our $Co_{1.8}$-HAlSiβ sample (**Table 5**, 0.86×10^{-3} s^{-1}). These samples were (i) evaluated in the ODHP reaction under close experimental conditions, (ii) both synthetized by

cationic exchange of the protons of beta zeolites exhibiting close Si/Al ratios (17.6 for Bulánek et al. [19] *vs* 13.6 in the present study, **Table 1**) and (iii) exhibited close Co loadings (1.68 wt% Co for Bulánek et al. [19] *vs* 1.82 wt% Co in the present study, **Table 1**). This remarkable agreement provides support for the reliability of the rates measured in the ODHP reaction in the present study. Overall, **Table 6** shows that the TOFs of the $Co_{1.9}$-Siβ-pH-2.5 sample are found to be greater than or equal to those reported in most of the earlier studies performed with Co-containing materials [17, 18, 20-28]. The fact that the TOF of $Co_{1.9}$-Siβ-pH-2.5 appears to be lower than those reported on Co supported on Zr molecular organic framework (NU1000 [29]) and carbon nanotubes (CNTs [30]), respectively, illustrates the crucial importance of the support in the ODHP reaction. Regarding the earlier studies performed on silica-based materials, the TOF of the $Co_{1.9}$-Siβ-pH-2.5 sample is found to be much higher than those reported in earlier studies [19, 23, 30] suggesting that the incorporation of the Co species into the framework of Siβ zeolite would be beneficial for the ODHP reaction.

4. Conclusion

The Co_x-Siβ (*x* being the Co weight loading) samples prepared by incorporation of Co^{2+} species in the silanol nests (created by dealumination of a HAlSiβ support) appeared to be about 4 times more active in the ODHP reaction on a TOF basis compared to a reference sample for which Co was located in cationic exchange positions of a HAlSiβ support. Despite obvious differences in Co speciation in solution between pH 2.5 and 9.0 (**Figure 2**), the change in pH during deposition of the Co^{2+} species in the silanol nests was found to have hardly any influence on the resulting ODHP catalytic activity below a Co loading of 5 wt%. This peculiarity was assigned to the transient

acidification of the medium to pH 3.0 with the addition of Siβ in the Co solution set originally at pH 9.0, and the rapid dissolution of the $Co(OH)_2$ precipitate and incorporation of the Co species in the Siβ framework. The fact that the TOF was found to remain essentially constant below 5 wt % of Co in the Co_x-Siβ series may be rather attributed to the maximum content of Co incorporable in the silanol nests created by dealumination of the HAlSiβ pristine support. The TOF of a $Co_{1.9}$-Siβ-pH-2.5 sample is found to be greater than or equal to those reported in most of the earlier studies performed with Co-containing materials and to be about 7 times greater than that of V-Siβ materials [36] under comparable experimental conditions in terms of O_2 and C_3H_8 concentrations in the reacting feed (**Table 6**). The latter illustrates the superiority of Co over V for the ODHP reaction when incorporated into the silanol nests of a dealuminated Siβ supporting oxide. Finally, this work paves the way for the characterization of the Co^{2+} species by NO-TPD. NO was found to be weakly chemisorbed on the Co^{2+} species and to be relatively sensitive to the Co environment as the NO/Co ratio was found to decrease as the loading of Co increased, however, whereas differences in Co dispersion could not be observed by XPS. Additional work is currently under progress on more model materials for the characterization of supported Co^{2+} species by NO-TPD.

CRediT author statement

Stanislaw Dzwigaj: Investigation, Resources, Writing – Review & Editing. **Diane Reja:** Investigation, Data Curation. **Saremblé Koné-Guira:** Investigation, Data Curation. **Antoine Miche:** Investigation, Data Curation. **Guylène Costentin:** Conceptualization, Writing – Review & Editing. **Cyril Thomas:** Conceptualization, Validation, Investigation, Resources, Data Curation,

Writing – Original Draft, Writing – Review & Editing, Visualization, Supervision, Project Administration. All co-authors have read and agreed on the submitted version of the manuscript.

Acknowledgments

The authors thank Sorbonne Université and CNRS for providing funding (Crédits récurrents) and access to the analytical equipment used in the present work. D.R. gratefully acknowledges Sorbonne Université for financial support (PhD Grant no 3892/2020). The authors also express their gratitude to J. Noël (Plateforme ALIPP6, Laboratoire d'Analyse Géochimie Elémentaire, Sorbonne Université) for her rigorous analysis of the ICP-OES data. Dr. C. Reynaud (Sorbonne Université, PhD Grant no 3415/2019) is acknowledged for the computation of the data regarding Co speciation in solution shown in **Figure 2**. The authors also acknowledge L. Anscieau for his help in recovering the original data of **Figure S5** that were stored in the hard disk drive of an out of order 27 years old PC.

Conflicts of interest

There is no conflict of interest to declare.

Table 1. Chemical composition of the samples determined by ICP-OES.

Samples	Targeted Co loading (wt%)	Element concentration			Si/Al at. ratio
		Si (wt%)	Al (wt%)	Co (wt%)	
HAlSiβ	-	37.63	2.65	-	13.6
$Co_{1.8}$-HAlSiβ	2.0	37.97	2.63	1.82	13.9
Siβ	-	42.00	0.11	-	380
$Co_{1.1}$-Siβ-pH-2.5	1.0	41.47	0.09	1.11	459
$Co_{1.9}$-Siβ-pH-2.5	2.0	43.02	0.09	1.89	470
$Co_{3.0}$-Siβ-pH-2.5	3.0	42.03	0.08	2.95	508
$Co_{5.6}$-Siβ-pH-2.5	5.0	40.92	0.08	5.64	501
$Co_{9.3}$-Siβ-pH-2.5	9.0	39.25	0.08	9.26	467
$Co_{0.9}$-Siβ-pH-9.0	1.0	44.15	0.07	0.93	579
$Co_{2.2}$-Siβ-pH-9.0	2.0	43.12	0.09	2.19	488
$Co_{3.1}$-Siβ-pH-9.0	3.0	42.32	0.09	3.07	469
$Co_{4.3}$-Siβ-pH-9.0	5.0	41.97	0.07	4.34	565
$Co_{9.3}$-Siβ-pH-9.0	9.0	39.43	0.08	9.28	487

Table 2. O 1s, C 1s, Al 2p and Co $2p_{3/2}$ binding energies referenced to Si 2p at 103.3 eV and Si/Al at. ratio.

	Binding energy (eV)				
Samples	O 1s	C 1s	Al 2p	Co $2p_{3/2}$	Si/Al at. ratio
HAlSiβ	532.6	284.4	74.5	-	15.3
$Co_{1.8}$-HAlSiβ	532.5	284.9	74.5	782.5	15.6
Siβ	532.6	283.9	*	-	-
$Co_{1.1}$-Siβ-pH-2.5	532.5	283.8	*	781.4	-
$Co_{1.9}$-Siβ-pH-2.5	532.5	283.8	*	781.2	-
$Co_{3.0}$-Siβ-pH-2.5	532.5	284.0	*	781.4	-
$Co_{5.6}$-Siβ-pH-2.5	532.5	284.3	*	781.3	-
$Co_{9.3}$-Siβ-pH-2.5	532.5	283.9	*	781.3	-
$Co_{0.9}$-Siβ-pH-9.0	532.5	284.0	*	781.3	-
$Co_{2.2}$-Siβ-pH-9.0	532.5	283.8	*	781.2	-
$Co_{3.1}$-Siβ-pH-9.0	532.6	285.0	*	781.8	-
$Co_{4.3}$-Siβ-pH-9.0	532.5	283.9	*	780.9	-
$Co_{9.3}$-Siβ-pH-9.0	532.5	283.9	*	780.8	-

*Absence of Al 2p signal measurable under the conditions used.

Table 3. Initial C_3H_8 conversion (X_{C3H8}^{i}) at 400 °C and C_3H_8 conversion at 400 °C after reaction at 500 °C (X_{C3H8}^{f}) together with the corresponding selectivity in C_3H_6 (S_{C3H6}^{i} and S_{C3H6}^{f}) in the C_3H_8 ODHP reaction (8.2 % C_3H_8 - 1.9 % O_2 - He, about 20 µmol Co in the sample weight (sw) of catalyst diluted in 600 mg α-Al_2O_3, 74.1 mL min^{-1} total flow rate) over various Co samples. X_{C3H8}^{diff} represents the evolution of the C_3H_8 conversion at 400 °C after reaction at 500 °C ($X_{C3H8}^{diff} = ((X_{C3H8}^{f} - X_{C3H8}^{i}) / X_{C3H8}^{i}) \times 100$).

	Co_x-Siβ-pH-2.5						Co_x-HAlSiβ						Co_x-Siβ-pH-9.0					
sw	*x*	X_{C3H8}^{i}	S_{C3H6}^{i}	X_{C3H8}^{f}	S_{C3H6}^{f}	X_{C3H8}^{diff}	*x*	X_{C3H8}^{i}	S_{C3H6}^{i}	X_{C3H8}^{f}	S_{C3H6}^{f}	X_{C3H8}^{diff}	*x*	X_{C3H8}^{i}	S_{C3H6}^{i}	X_{C3H8}^{f}	S_{C3H6}^{f}	X_{C3H8}^{diff}
(mg)	wt %	%	%	%	%	%	wt %	%	%	%	%	%	wt %	%	%	%	%	%
120	1.1	2.8	47	2.8	48	0							0.9	3.0	45	3.2	46	+ 6
60	1.9	3.7	36	2.9	47	- 22	1.8	0.8	67	0.6	60	- 25	2.2	2.4	47	2.7	49	+ 13
40	3.0	3.7	34	2.9	45	- 22							3.1	3.1	44	2.8	49	- 11
24	5.6	2.2	53	2.0	55	- 10							4.3	3.8	36	3.2	44	- 16
13	9.3	1.9	33	1.6	38	- 16							9.3	2.8	33	2.0	38	- 30

Table 4. Initial C_3H_6 concentration at 400 °C ($C_3H_6^i$) and C_3H_6 concentration at 400 °C after ODHP reaction at 500 °C ($C_3H_6^f$) (8.2 % C_3H_8 - 1.9 % O_2 - He, about 20 µmol Co diluted in 600 mg α-Al_2O_3, 74.1 mL min^{-1} total flow rate).

Co_x-Siβ-pH-2.5			Co_x-HAlSiβ			Co_x-Siβ-pH-9.0		
x wt%	$C_3H_6^i$ (ppm)	$C_3H_6^f$ (ppm)	*x* wt%	$C_3H_6^i$ (ppm)	$C_3H_6^f$ (ppm)	*x* wt%	$C_3H_6^i$ (ppm)	$C_3H_6^f$ (ppm)
1.1	1051	1085				0.9	976	1134
1.9	1079	1093	1.8	570	501	2.2	928	1067
3.0	1041	1105				3.1	900	1071
5.6	932	881				4.3	1095	1128
9.3	501	464				9.3	751	610

Table 5. Turnover frequency (TOF [54]) data calculated on the basis of the total number of Co atoms and on the amount of C_3H_6 produced at 400 °C after ODHP reaction at 500 °C (8.2 % C_3H_8 - 1.9 % O_2 - He, about 20 μmol Co diluted in 600 mg α-Al_2O_3, 74.1 mL min^{-1} total flow rate).

	TOF (x 10^3 s^{-1})		TOF (x 10^3 s^{-1})		TOF (x 10^3 s^{-1})
x	Co_x-Siβ-pH-2.5	*x*	Co_x-HAlSiβ	*x*	Co_x-Siβ-pH-9.0
1.1	2.65			0.9	3.47
1.9	3.13	1.8	0.86	2.2	2.64
3.0	3.04			3.1	3.01
5.6	2.11			4.3	3.52
9.3	1.21			9.3	1.60

Table 6. Comparison of the turnover frequencies (TOFs, molecule C_3H_6 s^{-1} Co or V $atom^{-1}$) reported in earlier studies with that measured in the present work on $Co_{1.9}$-Siβ-pH-2.5. These TOF calculated on a per atom basis were either extracted as is from the corresponding studies[i] or estimated from the data reported in these earlier works[j].

Sample	Co or V (wt%)	sw[a] (mg)	$[C_3H_8]$[b] (%)	$[O_2]$[c] (%)	F[d] (mL/min)	T[e] (°C)	X C_3H_8[f] (%)	S C_3H_6[g] (%)	TOF[h] (x 10^3 s^{-1})	Refs.
Co-AIM + NU1000	-	80-100	3.0	10.0	-	230	-	-	0.28 [i]	[29]
Co/ZrO_2	-	-	3.0	10.0	-	230	-	-	0.04 [i]	[29]
$Co_{1.9}$-Siβ-pH-2.5	1.89	60	8.2	1.9	74.1	**230**	-	-	0.02 [k]	This work
$CeCo_{0.5}O_y$	9.72	100	5.0	15.0	100	300	-	-	0.25 [j]	[18]
$Co_{1.9}$-Siβ-pH-2.5	1.89	60	8.2	1.9	74.1	**300**	-	-	0.21 [k]	This work
$Cs_{2.5}H_{6x-0.5}Co_{1-x}PV_1Co_xMo_{11-x}O_{40}$	2.81	500-750	40.0	20.0	15	345	5.0	79.1	0.74-0.49 [j]	[20]
$Co_{1.9}$-Siβ-pH-2.5	1.89	60	8.2	1.9	74.1	**345**	-	-	0.79 [k]	This work
CoOx-CNTs	0.49	-	16.7	16.7	30	353	-	71	94.55 [j]	[30]
$Co_{1.9}$-Siβ-pH-2.5	1.89	60	8.2	1.9	74.1	**353**	-	-	0.98 [k]	This work
CoOx-MCM-41	0.49	-	16.7	16.7	30	393	-	-	0.70 [j]	[30]
CoOx-SiO_2	0.49	-	16.7	16.7	30	393	-	-	0.33 [j]	[30]
CoH-BEA-17.5-0.42	1.68	200	5.0	6.5	100	400	3.9	29.4	0.75 [k]	[19]
$CoMO\phi y$ ($CoMoO_4$)	26.9	200	29.0	14.9	20	400	8.8	46.4	0.19 [j]	[26]
$Co^{III}_{0.36}Co^{II}_{0.30}Al_{0,34}(PO_4)_{0.11}O_{1.19}$	50.1	100	16.7	16.7	50	400	27.9	36.0	0.73 [j]	[28]
$Co_{1.9}$-Siβ-pH-2.5	1.89	60	8.2	1.9	74.1	**400**	2.9	46.8	3.13	This work
$V_{0.25}$-Siβ	0.25	200	6.6	2.1	15	400	1.3	34.1	0.4 [i]	[36]
Co36SrHAp	1.42	500	14.3	4.0	30	450	15.8	46.6	1.95 [j]	[21]

Co_2O_3/SiO_2	3.55	1000	18.1	18.1	83	450	15.8	15.8	0.46 [j]	[23]
CoMgAlO	9.67	-	-	-	-	450	1.5	92.5	0.33 [j]	[24]
$Co_{1.9}$-Siβ-pH-2.5	1.89	60	8.2	1.9	74.1	**450**	-	-	9.13 [k]	This work
$CoWO_4$	19.2	1000	15.0	15.0	60	500	12.6	38.5	0.10 [j]	[17]
Co_2B/Co_3B	93.2	235	30.0	15.0	50-160	500	13-23	88.2	0.36 [j]	[27]
P(0.05)CoO	69.4	100	11.8	9.8	50	500	27.2	53.8	0.55 [j]	[25]
$Co_{1.9}$-Siβ-pH-2.5	1.89	60	8.2	1.9	74.1	**500**	-	-	23.18 [k]	This work
CoMOϕx ($CoMoO_4$)	29.8	1000	29.0	14.9	100	600	15.0	38.5	0.25 [j]	[22]
$Co_{1.9}$-Siβ-pH-2.5	1.89	60	8.2	1.9	74.1	**600**	-	-	108.50 [k]	This work

[a] sample weight, [b] C_3H_8 concentration in the feed as vol. %, [c] O_2 concentration in the feed as vol. %,[d] even though in most studies the fact that the flow rates were not explicitly defined in the normal conditions (i.e. 273 K and 1 atm), the reported flow rates were considered as such for the estimation of the TOF, [e] reaction temperature, [f] conversion of C_3H_8, [g] Selectivity in C_3H_6, [h] TurnOver Frequency on a per cobalt atom basis, TOF extracted as is from the corresponding studies[i] or estimated from the data reported in these earlier works[j], [k] TOF values extrapolated at the corresponding temperatures from the TOF estimated at 400 °C (3.13×10^{-3} s^{-1}) and considering an activation energy of 86.6 kJ/mol (Figure S8a).

Figure Captions:

Figure 1. NO_x profiles recorded by chemiluminescence analyzers (Thermo Environmental Instruments 42C-HL (red trace) or Eco Physics CLD 700 AL (black trace)) on about 0.12 g of $Co_{1.1}$Siβ-pH-2.5 after annealing of the sample at 500 °C for 2 h in 100 mL_{NTP}/min of He or Ar and RT exposure to 230 mL_{NTP}/min of NO (400 ppm) in He or Ar for 2 h, followed by temperature-programmed desorption from RT to 400 °C (3 °C/min) in 230 mL_{NTP}/min of He or Ar.

Figure 2 Speciation of Co as a function of the pH of the aqueous medium for Co precursor concentrations of (a) 1.6 and (b) 17.4 x 10^{-3} mol/L. Dotted lines put emphasis on the Co species present at pH 2.5 and 9.0.

Figure 3. Co $2p_{3/2}$/Si 2p surface at. (XPS) ratios as a function of the bulk (ICP-OES) ones. Co_x-Siβ-pH-2.5 (○), Co_x-Siβ-pH-9.0 (●) and $Co_{1.8}$-HAlSiβ (●).

Figure 4. H_2-TPR profiles recorded from RT to 900 °C in 5% H_2/Ar with a 25 mL/min flow rate and a heating rate of 10 °C/min on (a) Co_x-Siβ-pH-2.5 and (b) Co_x-Siβ-pH-9.0 previously calcined at 500 °C (10 °C/min) under 5%O_2/He for 1 h. It must be noted that the H_2-TPR profile could not be recorded on $Co_{9.3}$-Siβ-pH-2.5 because of an experimental issue in the course of the H_2-TPR experiment on the last aliquot of the corresponding sample.

Figure 5. NO-TPD profiles recorded on (a) HAlSiβ and $Co_{1.8}$-HAlSiβ, (b) Co_x-Siβ-pH-2.5 and (c) Co_x-Siβ-pH-9.0 after annealing of the samples at 500 °C for 2 h in 100 mL_{NTP} min^{-1} of He or Ar and RT exposure to 230 mL_{NTP} min^{-1} of NO(400 ppm) in He or Ar for 2 h followed by temperature-programmed desorption from RT to 500 °C (3 °C min^{-1}) in 230 mL_{NTP} min^{-1} of He or Ar. (d) NO uptakes deduced from the corresponding NO-TPD profiles and (e) NO/Co ratios for Co_x-Siβ-pH-2.5 and Co_x-Siβ-pH-9.0 samples.

Figure 6. Evolution of the conversion of C_3H_8 (black trace) and the concentrations in C_3H_6 (blue trace), O_2 (red trace) and CO_x (gray trace) (8.2% C_3H_8, 1.9% O_2 in He, 74.1 mL_{NTP} min^{-1} total flow) in the ODHP reaction as a function of time on stream and reacting temperature on 60 mg of catalyst diluted in 600 mg of α-Al_2O_3, (a) $Co_{1.9}$-Siβ-pH-2.5, (b) $Co_{2.2}$-Siβ-pH-9.0 and (c) $Co_{1.8}$-HAlSiβ. The numbers reported on the figures are related to the reaction temperature.

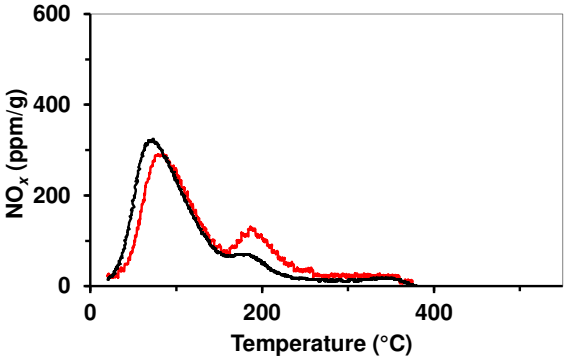

Figure 1. NO_x profiles recorded by chemiluminescence analyzers (Thermo Environmental Instruments 42C-HL (red trace) or Eco Physics CLD 700 AL (black trace)) on about 0.12 g of $Co_{1.1}Si\beta$-pH-2.5 after annealing of the sample at 500 °C for 2 h in 100 mL_{NTP}/min of He or Ar and RT exposure to 230 mL_{NTP}/min of NO (400 ppm) in He or Ar for 2 h, followed by temperature-programmed desorption from RT to 400 °C (3 °C/min) in 230 mL_{NTP}/min of He or Ar.

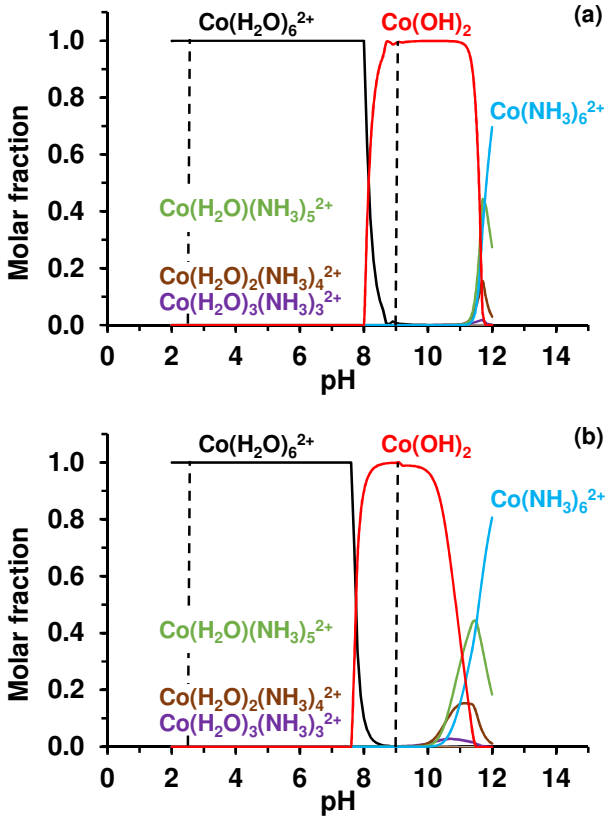

Figure 2. Speciation of Co as a function of the pH of the aqueous medium for Co precursor concentrations of (a) 1.6 and (b) 17.4 x 10^{-3} mol/L. Dotted lines put emphasis on the Co species present at pH 2.5 and 9.0.

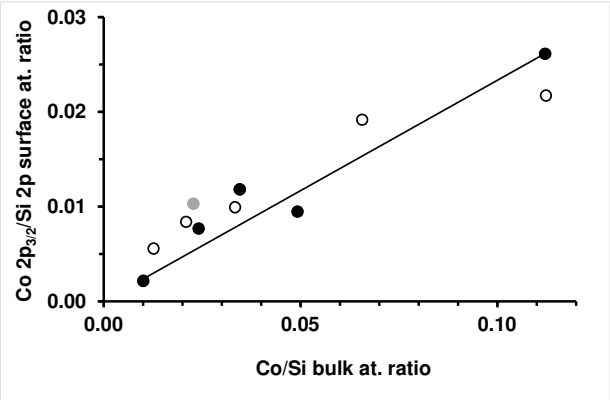

Figure 3. Co $2p_{3/2}$/Si 2p surface at. (XPS) ratios as a function of the bulk (ICP-OES) ones. Co_x-Siβ-pH-2.5 (○), Co_x-Siβ-pH-9.0 (●) and $Co_{1.8}$-HAlSiβ (●).

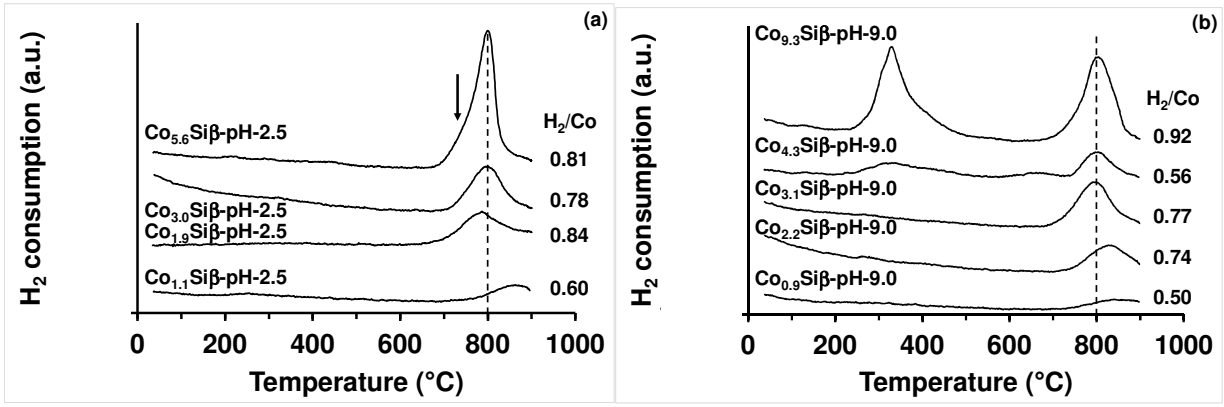

Figure 4. H_2-TPR profiles recorded from RT to 900 °C in 5% H_2/Ar with a 25 mL/min flow rate and a heating rate of 10 °C/min on (a) Co_x-Siβ-pH-2.5 and (b) Co_x-Siβ-pH-9.0 previously calcined at 500 °C (10 °C/min) under 5%O_2/He for 1 h. It must be noted that the H_2-TPR profile could not be recorded on $Co_{9.3}$-Siβ-pH-2.5 because of an experimental issue in the course of the H_2-TPR experiment on the last aliquot of the corresponding sample.

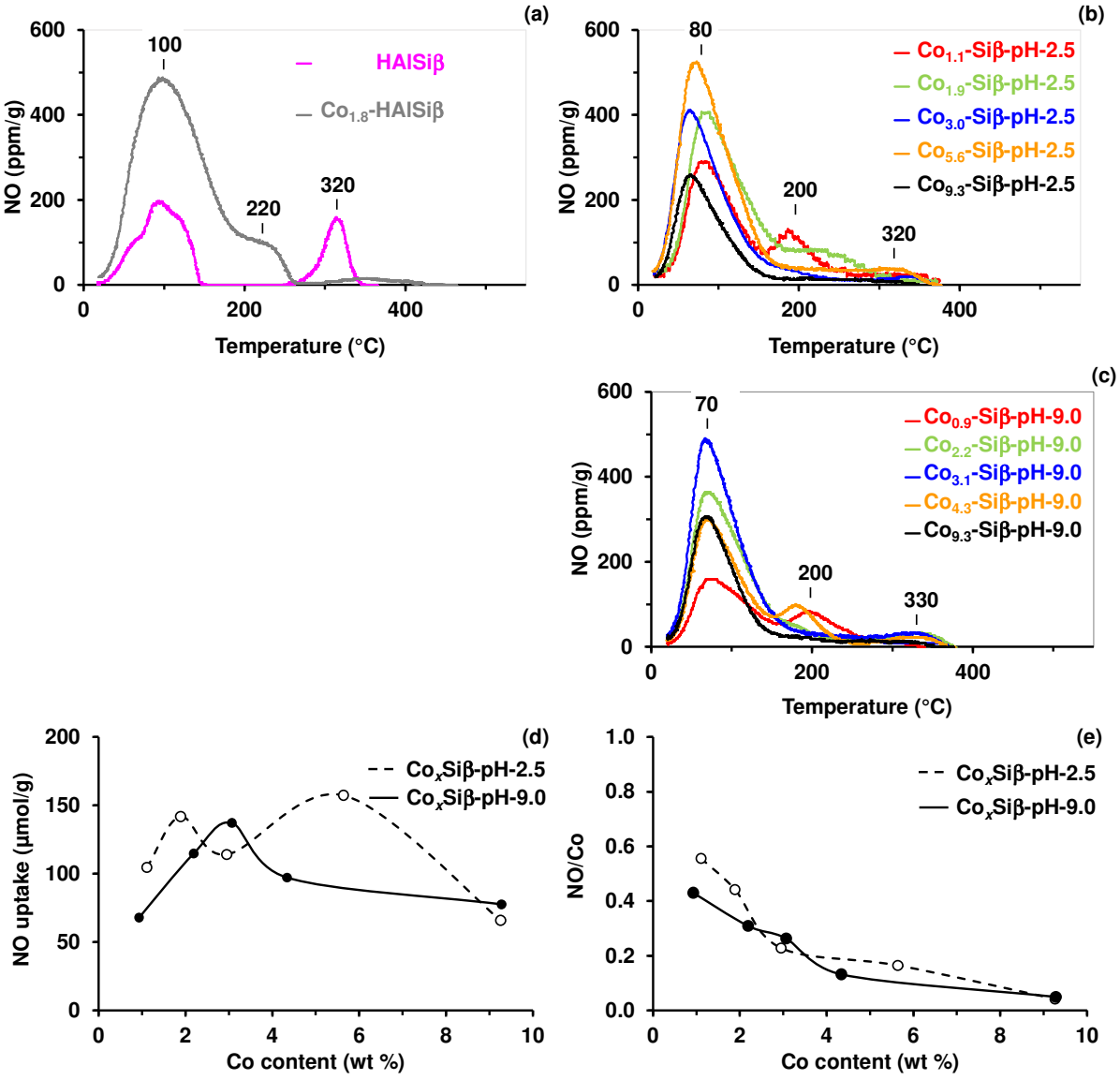

Figure 5. NO-TPD profiles recorded on (a) HAlSiβ and $Co_{1.8}$-HAlSiβ, (b) Co_x-Siβ-pH-2.5 and (c) Co_x-Siβ-pH-9.0 after annealing of the samples at 500 °C for 2 h in 100 mL_{NTP} min^{-1} of He or Ar and RT exposure to 230 mL_{NTP} min^{-1} of NO(400 ppm) in He or Ar for 2 h, followed by temperature-programmed desorption from RT to 500 °C (3 °C min^{-1}) in 230 mL_{NTP} min^{-1} of He or Ar. (d) NO uptakes deduced from the corresponding NO-TPD profiles and (e) NO/Co ratios for Co_x-Siβ-pH-2.5 and Co_x-Siβ-pH-9.0 samples.

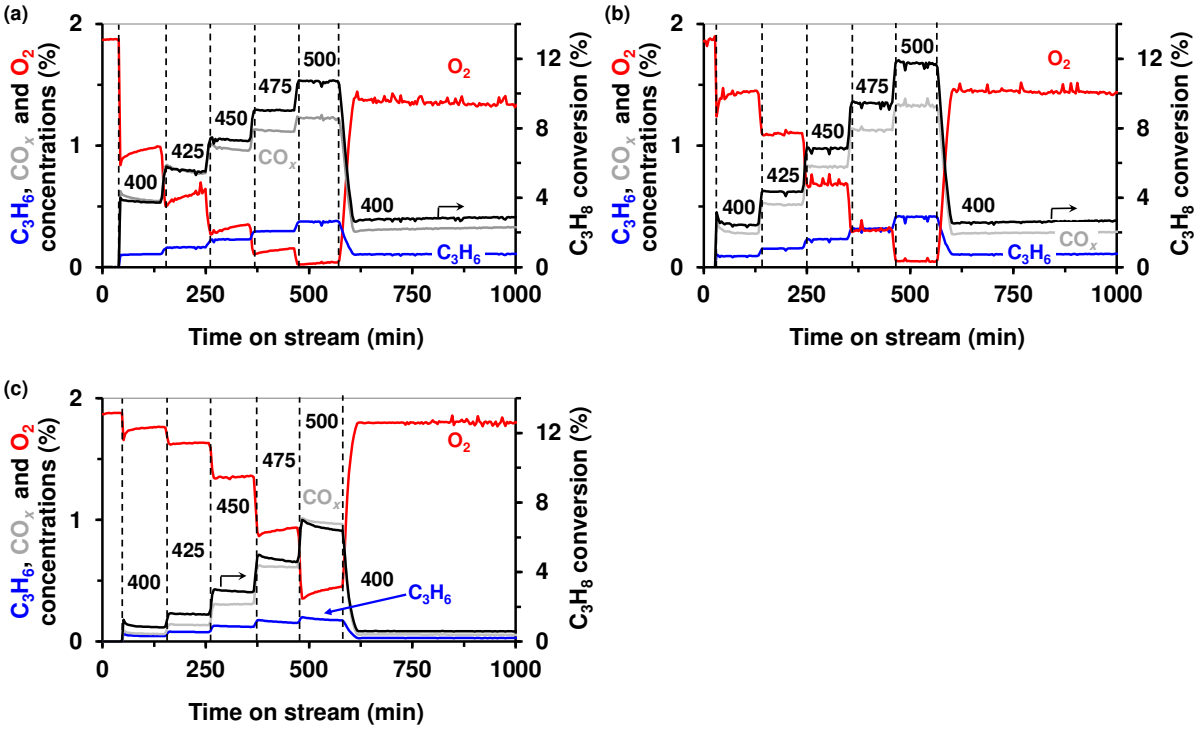

Figure 6. Evolution of the conversion of C_3H_8 (black trace) and the concentrations in C_3H_6 (blue trace), O_2 (red trace) and CO_x (gray trace) (8.2% C_3H_8, 1.9% O_2 in He, 74.1 mL_{NTP} min^{-1} total flow) in the ODHP reaction as a function of time on stream and reacting temperature on 60 mg of catalyst diluted in 600 mg of α-Al_2O_3, (a) $Co_{1.9}$-Siβ-pH-2.5, (b) $Co_{2.2}$-Siβ-pH-9.0 and (c) $Co_{1.8}$-HAlSiβ. The numbers reported on the figures are related to the reaction temperature.

References

[1] C.A. Carrero, R. Schlögl, I.E. Wachs, R. Schomaecker, Critical literature review of the kinetics for the oxidative dehydrogenation of propane over well-defined supported vanadium oxide catalysts, ACS Catal., 4 (2014) 3357-3380. https://doi.org/3310.1021/cs5003417.

[2] F. Cavani, N. Ballarini, A. Cericola, Oxidative dehydrogenation of ethane and propane: How far from commercial implementation?, Catal. Today, 127 (2007) 113-131. https://doi.org/110.1016/j.cattod.2007.1005.1009.

[3] J.T. Grant, J.M. Venegas, W.P. McDermott, I. Hermans, Aerobic oxidations of light alkanes over solid metal oxide catalysts, Chem. Rev., 118 (2018) 2769-2815. https://doi.org/2710.1021/acs.chemrev.2767b00236.

[4] Y. Gambo, S. Adamu, A.A. Abdulrasheed, R.A. Lucky, M.S. Ba-Shammakh, M.M. Hossain, Catalyst design and tuning for oxidative dehydrogenation of propane–A review, Appl. Catal. A: General, 609 (2021) 117914. https://doi.org/117910.111016/j.apcata.112020.117914.

[5] S. Dong, N.R. Altvater, L.O. Mark, I. Hermans, Assessment and comparison of ordered & non-ordered supported metal oxide catalysts for upgrading propane to propylene, Appl. Catal. A: General, 617 (2021) 118121. https://doi.org/118110.111016/j.apcata.112021.118121.

[6] J. Bricker, History and state of the art of ethane/propane dehydrogenation catalysis, Board on Chemical Sciences and Technology Workshop on The Changing Landscape of Hydrocarbon Feedstocks for Chemical Production: Implications for Catalysis, Washington, DC, 2016.

[7] J.A. Loiland, Z. Zhao, A. Patel, P. Hazin, Boron-containing catalysts for the oxidative dehydrogenation of ethane/propane mixtures, Ind. Eng. Chem. Res., 58 (2019) 2170-2180. https://doi.org/2110.1021/acs.iecr.2178b04906.

[8] J.S. Valente, R. Quintana-Solórzano, H.c. Armendáriz-Herrera, J.-M.M. Millet, Decarbonizing petrochemical processes: contribution and perspectives of the selective oxidation of C1–C3 paraffins, ACS Catal., 13 (2023) 1693-1716. https://doi.org/1610.1021/acscatal.1692c05161.

[9] S. Chen, X. Chang, G. Sun, T. Zhang, Y. Xu, Y. Wang, C. Pei, J. Gong, Propane dehydrogenation: catalyst development, new chemistry, and emerging technologies, Chem. Soc. Rev., 50 (2021) 3315-3354. https://doi.org/3310.1039/D3310CS00814A.

[10] A. Iglesias-Juez, A.M. Beale, K. Maaijen, T.C. Weng, P. Glatzel, B.M. Weckhuysen, A combined in situ time-resolved UV–Vis, Raman and high-energy resolution X-ray absorption spectroscopy study on the deactivation behavior of Pt and PtSn propane dehydrogenation catalysts under industrial reaction conditions, J. Catal., 276 (2010) 268-279. https://doi.org/210.1016/j.jcat.2010.1009.1018.

[11] J. Grant, C.A. Carrero, F. Goeltl, J. Venegas, P. Mueller, S.P. Burt, S. Specht, W. McDermott, A. Chieregato, I. Hermans, Selective oxidative dehydrogenation of propane to propene using boron nitride catalysts, Science, 354 (2016) 1570-1573. https://doi.org/1510.1126/science.aaf7885.

[12] J.M. Venegas, Z. Zhang, T.O. Agbi, W.P. McDermott, A. Alexandrova, I. Hermans, Why boron nitride is such a selective catalyst for the oxidative dehydrogenation of propane, Angew. Chem. Inter. Ed., 59 (2020) 16527-16535. https://doi.org/16510.11002/anie.202003695.

[13] P. Mars, D.W. Van Krevelen, Oxidations carried out by means of vanadium oxide catalysts, Chem. Eng. Sci., 3 (1954) 41-59. https://doi.org/10.1016/S0009-2509(1054)80005-80004.

[14] S. Albonetti, F. Cavani, F. Trifiro, Key aspects of catalyst design for the selective oxidation of paraffins, Catal. Rev., 38 (1996) 413-438. https://doi.org/410.1080/01614949608006463.

[15] M. Chaar, D. Patel, H. Kung, Selective oxidative dehydrogenation of propane over V-Mg-O catalysts, J. Catal., 109 (1988) 463-467. https://doi.org/410.1016/0021-9517(1088)90226-90226.

[16] T. Blasco, J.L. Nieto, Oxidative dehydrogenation of short chain alkanes on supported vanadium oxide catalysts, App. Catal. A: General, 157 (1997) 117-142. https://doi.org/110.1016/S0926-1860X(1097)00029-X.

[17] D.L. Stern, R.K. Grasselli, Propane oxydehydrogenation over metal tungstates, J. Catal., 167 (1997) 570-572. https://doi.org/510.1006/jcat.1997.1570.
[18] L. Jalowiecki-Duhamel, A. Ponchel, C. Lamonier, A. D'Huysser, Y. Barbaux, Relationship between structure of $CeNi_XO_Y$ mixed oxides and catalytic properties in oxidative dehydrogenation of propane, Langmuir, 17 (2001) 1511-1517. https://doi.org/1510.1021/la001103y.
[19] R. Bulánek, K. Novoveská, B. Wichterlová, Oxidative dehydrogenation and ammoxidation of ethane and propane over pentasil ring Co-zeolites, Appl. Catal. A: General, 235 (2002) 181-191. https://doi.org/110.1016/S0926-1860X(1002)00263-00266.
[20] N. Dimitratos, J.C. Védrine, Role of acid and redox properties on propane oxidative dehydrogenation over polyoxometallates, Catal. Today, 81 (2003) 561-571. https://doi.org/510.1016/S0920-5861(1003)00154-00158.
[21] S. Sugiyama, T. Shono, D. Makino, T. Moriga, H. Hayashi, Enhancement of the catalytic activities in propane oxidation and H–D exchangeability of hydroxyl groups by the incorporation with cobalt into strontium hydroxyapatite, J. Catal., 214 (2003) 8-14. https://doi.org/10.1016/S0021-9517(1002)00101-X.
[22] L.A. Palacio, A. Echavarría, L. Sierra, E.A. Lombardo, Cu, Mn and Co molybdates derived from novel precursors catalyze the oxidative dehydrogenation of propane, Catal. Today, 107 (2005) 338-345. https://doi.org/310.1016/j.cattod.2005.1007.1031.
[23] B.Y. Jibril, M.C. Al-Kinany, S.H. Al-Khowaiter, S.A. Al-Drees, H.A. Al-Megren, M.A. Al-Dosari, R.H. Al-Rasheed, S.M. Al-Zahrani, A.E. Abasaeed, Performances of new kieselguhr-supported transition metal oxide catalysts in propane oxydehydrogenation, Catal. Comm., 7 (2006) 79-85. https://doi.org/10.1016/j.catcom.2005.1008.1014.
[24] S. Tanasoi, G. Mitran, N. Tanchoux, T. Cacciaguerra, F. Fajula, I. Săndulescu, D. Tichit, I.-C. Marcu, Transition metal-containing mixed oxides catalysts derived from LDH precursors for short-chain hydrocarbons oxidation, Appl. Catal. A: General, 395 (2011) 78-86. https://doi.org/10.1016/j.apcata.2011.1001.1028.
[25] X.-Z. Lin, G.-C. Li, C.-J. Huang, W.-Z. Weng, H.-L. Wan, P-Modified cobalt oxide: A novel and effective catalyst for oxidative dehydrogenation of propane, Chinese Chem. Lett., 24 (2013) 789-792. https://doi.org/710.1016/j.cclet.2013.1005.1013.
[26] J. Velasquez, A. Echavarria, A. Faro, L.A. Palacio, Propane oxidative dehydrogenation on ZnCoMo and NiCoMo catalysts obtained from *ϕy* and *ϕx* precursors, Ind. Eng. Chem. Res., 52 (2013) 5582-5586. https://doi.org/5510.1021/ie3025856.
[27] J.T. Grant, W.P. McDermott, J.M. Venegas, S.P. Burt, J. Micka, S.P. Phivilay, C.A. Carrero, I. Hermans, Boron and boron-containing catalysts for the oxidative dehydrogenation of propane, ChemCatChem, 9 (2017) 3623-3626. https://doi.org/3610.1002/cctc.201701140.
[28] M.-X. Huang, X. Wu, X.-D. Yi, G.-B. Han, W.-S. Xia, H.-L. Wan, Highly dispersed CoO_x in layered double oxides for oxidative dehydrogenation of propane: guest–host interactions, RSC adv., 7 (2017) 14846-14856. https://doi.org/14810.11039/C14847RA01190C.
[29] Z. Li, A.W. Peters, V. Bernales, M.A. Ortuño, N.M. Schweitzer, M.R. DeStefano, L.C. Gallington, A.E. Platero-Prats, K.W. Chapman, C.J. Cramer, Metal–Organic Framework supported cobalt catalysts for the oxidative dehydrogenation of propane at low temperature, ACS Cent. Sci., 3 (2017) 31-38. https://doi.org/10.1021/acscentsci.1026b00290.
[30] H. Zhou, H. Lou, W. Lu, Improving the catalytic efficiency of carbon-based active sites by trace oxide promoters for highly productive olefin synthesis, Catal. Sci. Technol., 7 (2017) 802-806. https://doi.org/810.1039/C1036CY02562E.
[31] R.J. Saxton, W. Chester, J.G. Zajacek, G.L. Crocco, US Pat. 5 374 747, (1994).
[32] G.-J. Kim, D.-S. Cho, K.-H. Kim, W.-S. Ko, J.-H. Kim, H. Shoji, Incorporation of vanadium into the mordenite structure by direct hydrothermal crystallization and secondary synthesis, Catal. Lett., 31 (1995) 91-102. https://doi.org/110.1007/BF00817036.

[33] B. Kraushaar, J. Van Hooff, A new method for the preparation of titanium-silicalite (TS-1), Catal. Lett., 1 (1988) 81-84. https://doi.org/10.1007/BF00772769.
[34] S. Dzwigaj, M. Peltre, P. Massiani, A. Davidson, M. Che, T. Sen, S. Sivasanker, Incorporation of vanadium species in a dealuminated β zeolite, Chem. Comm., (1998) 87-88. https://doi.org/10.1039/A704556E.
[35] I.C. Medeiros-Costa, E. Dib, N. Nesterenko, J.-P. Dath, J.-P. Gilson, S. Mintova, Silanol defect engineering and healing in zeolites: Opportunities to fine-tune their properties and performances, Chem. Soc. Rev., 50 (2021) 11156-11179. https://doi.org/11110.11039/D11151CS00395J.
[36] K. Chalupka, C. Thomas, Y. Millot, F. Averseng, S. Dzwigaj, Mononuclear pseudo-tetrahedral V species of VSiBEA zeolite as the active sites of the selective oxidative dehydrogenation of propane, J. Catal., 305 (2013) 46-55. http://dx.doi.org/10.1016/j.jcat.2013.1004.1020.
[37] S. Dzwigaj, M. Che, Incorporation of Co (II) in dealuminated BEA zeolite at lattice tetrahedral sites evidenced by XRD, FTIR, diffuse reflectance UV− Vis, EPR, and TPR, J. Phys. Chem. B, 110 (2006) 12490-12493. https://doi.org/12410.11021/jp0623387.
[38] A. Mihaylova, K. Hadjiivanov, S. Dzwigaj, M. Che, Remarkable effect of the preparation technique on the state of cobalt ions in BEA zeolites evidenced by FTIR spectroscopy of adsorbed CO and NO, TPR and XRD, J. Phys. Chem. B, 110 (2006) 19530-19536. https://doi.org/19510.11021/jp0634398.
[39] R. Baran, T. Onfroy, S. Casale, S. Dzwigaj, Introduction of Co into the vacant T-atom sites of SiBEA zeolite as isolated mononuclear Co species, J. Phys. Chem. C, 118 (2014) 20445-20451. https://doi.org/20410.21021/jp506375v.
[40] R. Sadek, K. Chalupka-Spiewak, J.-M. Krafft, Y. Millot, L. Valentin, S. Casale, J. Gurgul, S. Dzwigaj, The synthesis of different series of cobalt BEA zeolite catalysts by post-synthesis methods and their characterization, Catalysts, 12 (2022) 1644. https://doi.org/1610.3390/catal12121644.
[41] J. Janas, T. Machej, J. Gurgul, R.P. Socha, M. Che, S. Dzwigaj, Effect of Co content on the catalytic activity of CoSiBEA zeolite in the selective catalytic reduction of NO with ethanol: Nature of the cobalt species, Appl. Catal. B: Environmental, 75 (2007) 239-248. https://doi.org/210.1016/j.apcatb.2007.1007.1029.
[42] P. Boroń, L. Chmielarz, S. Casale, C. Calers, J.-M. Krafft, S. Dzwigaj, Effect of Co content on the catalytic activity of CoSiBEA zeolites in N_2O decomposition and SCR of NO with ammonia, Catal. Today, 258 (2015) 507-517. http://dx.doi.org/510.1016/j.cattod.2014.1012.1001.
[43] P. Boroń, L. Chmielarz, B. Gil, B. Marszałek, S. Dzwigaj, Experimental evidence of NO SCR mechanism in the presence of the BEA Zeolite with framework and extra-framework cobalt species, Appl. Catal. B: Environmental, 198 (2016) 457-470. https://doi.org/410.1016/j.apcatb.2016.1006.1012.
[44] R. Baran, J.-M. Krafft, T. Onfroy, T. Grzybek, S. Dzwigaj, Influence of the nature and environment of cobalt on the catalytic activity of Co-BEA zeolites in selective catalytic reduction of NO with ammonia, Microporous Mesoporous Mater., 225 (2016) 515-523. https://doi.org/510.1016/j.micromeso.2015.1012.1061.
[45] A. Śrębowata, R. Baran, I.I. Kamińska, T. Onfroy, J.-M. Krafft, S. Dzwigaj, Catalytic hydrogen-assisted dehydrochlorination of 1, 2-dichloroethane over cobalt-containing beta zeolite, Catal. Today, 251 (2015) 73-80. https://doi.org/10.1016/j.cattod.2014.1010.1019.
[46] R. Sadek, K.A. Chalupka, P. Mierczynski, J. Rynkowski, J. Gurgul, S. Dzwigaj, Cobalt based catalysts supported on two kinds of beta zeolite for application in Fischer-Tropsch synthesis, Catalysts, 9 (2019) 497. https://doi.org/410.3390/catal9060497.
[47] R. Sadek, K.A. Chalupka, P. Mierczynski, J. Rynkowski, Y. Millot, L. Valentin, S. Casale, S. Dzwigaj, Fischer-Tropsch reaction on Co-containing microporous and mesoporous Beta zeolite catalysts: The effect of porous size and acidity, Catal. Today, 354 (2020) 109-122. https://doi.org/110.1016/j.cattod.2019.1005.1004.

[48] S. Dzwigaj, P. Massiani, A. Davidson, M. Che, Role of silanol groups in the incorporation of V in β zeolite, J. Mol. Catal. A: Chemical, 155 (2000) 169-182. https://doi.org/110.1016/S1381-1169(1099)00332-00335.
[49] G. Greczynski, L. Hultman, X-ray photoelectron spectroscopy: Towards reliable binding energy referencing, Prog. Mater. Sci., 107 (2020) 100591. https://doi.org/100510.101016/j.pmatsci.102019.100591.
[50] D. Kubička, N. Kumar, T. Venäläinen, H. Karhu, I. Kubičková, H. Österholm, D.Y. Murzin, Metal–support interactions in zeolite-supported noble metals: Influence of metal crystallites on the support acidity, J. Phys. Chem. B, 110 (2006) 4937-4946. https://doi.org/4910.1021/jp055754k.
[51] R.B. Borade, A. Clearfield, Characterization of acid sites in beta and ZSM-20 zeolites, J. Phys. Chem., 96 (1992) 6729-6737. https://doi.org/6710.1021/j100195a100037.
[52] J.H. Scofield, Hartree-Slater subshell photoionization cross-sections at 1254 and 1487 eV, J. Electron Spectrosc. Relat. Phenom., 8 (1976) 129-137. https://doi.org/110.1016/0368-2048(1076)80015-80011.
[53] W. Addison, R. Barrer, Sorption and reactivity of nitrous oxide and nitric oxide in crystalline and amorphous siliceous sorbents, J. Chem. Soc., (1955) 757-769. https://doi.org/710.1039/JR9550000757.
[54] S. Kozuch, J.M.L. Martin, "Turning Over" definitions in catalytic cycles, ACS Catal., 2 (2012) 2787-2794. https://doi.org/2710.1021/cs3005264.
[55] PHREEQC Version 3, U.S. Geological Survey - USGS, (2021). https://www.usgs.gov/software/phreeqc-version-3.
[56] B. Hu, N.M. Schweitzer, U. Das, H. Kim, J. Niklas, O. Poluektov, L.A. Curtiss, P.C. Stair, J.T. Miller, A.S. Hock, Selective propane dehydrogenation with single-site CoII on SiO_2 by a non-redox mechanism, J. Catal., 322 (2015) 24-37. https://doi.org/10.1016/j.jcat.2014.1010.1018.
[57] S. Dzwigaj, J. Janas, T. Machej, M. Che, Selective catalytic reduction of NO by alcohols on Co-and Fe-Siβ catalysts, Catal. Today, 119 (2007) 133-136. https://doi.org/110.1016/j.cattod.2006.1008.1055.
[58] D. Esquivel, A.J. Cruz-Cabeza, C. Jiménez-Sanchidrián, F.J. Romero-Salguero, Local environment and acidity in alkaline and alkaline-earth exchanged β zeolite: Structural analysis and catalytic properties, Microporous Mesoporous Mater., 142 (2011) 672-679. https://doi.org/610.1016/j.micromeso.2011.1001.1018.
[59] A.L.C. Pereira, J.M. González-Carballo, F.J. Pérez-Alonso, S. Rojas, J.L.G. Fierro, M.d.C. Rangel, Effect of the mesostructuration of the Beta zeolite support on the properties of cobalt catalysts for Fischer–Tropsch synthesis, Topics Catal., 54 (2011) 179-189. https://doi.org/110.1007/s11244-11011-19637-11246.
[60] A. Boix, J.G. Fierro, X-ray photoelectron spectroscopy analysis of platinum-and/or cobalt-loaded zeolites relevant for selective catalytic reduction of NO_x, Surf. Interface Anal., 27 (1999) 1107-1113. https://doi.org/1110.1002/(SICI)1096-9918(199912)199927:199912<191107::AID-SIA199685>199913.199910.CO;199912-O.
[61] M. Mhamdi, E. Marceau, S. Khaddar-Zine, A. Ghorbel, M. Che, Y. Ben Taarit, F. Villain, Preparation of Co^{2+}/ZSM5 catalysts by solid-state reaction: Influence of the precursor on cobalt speciation, Z. Phy. Chem., 219 (2005) 963-978. https://doi.org/910.1524/zpch.1219.1527.1963.67087.
[62] X. Wang, H.-Y. Chen, W.M.H. Sachtler, Catalytic reduction of NO_x by hydrocarbons over Co/ZSM-5 catalysts prepared with different methods, Appl. Catal. B: Environmental, 26 (2000) L227-L239. https://doi.org/210.1016/S0926-3373(1000)00125-00129.
[63] W. Li, S.Y. Yu, G.D. Meitzner, E. Iglesia, Structure and properties of cobalt-exchanged H-ZSM5 catalysts for dehydrogenation and dehydrocyclization of alkanes, J. Phys Chem. B, 105 (2001) 1176-1184. https://doi.org/1110.1021/jp002102h.
[64] Y. Li, J.N. Armor, Selective catalytic reduction of NO_x with methane over metal exchange zeolites, Appl. Catal. B: Environmental, 1993, pp. 239-256. https://doi.org/210.1016/0926-3373(1093)80051-E.

[65] L.B. Gutierrez, E.E. Miró, M.A. Ulla, Effect of the location of cobalt species on NO adsorption and NO_x-SCR over Co–mordenite, Appl. Catal. A: General, 321 (2007) 7-16. https://doi.org/10.1016/j.apcata.2006.1012.1022.
[66] J. Zhang, W. Fan, Y. Liu, R. Li, Synthesis and catalytic property of a Co^{2+}-exchanged Beta/Y composite for the selective catalytic reduction of NO by CH_4 in the presence of excess oxygen, Appl. Catal. B: Environmental, 76 (2007) 174-184. https://doi.org/110.1016/j.apcatb.2007.1005.1021.
[67] M. Ogura, M. Hayashi, S. Kage, M. Matsukata, E. Kikuchi, Determination of active palladium species in ZSM-5 zeolite for selective reduction of nitric oxide with methane, Appl. Catal. B: Environmental, 23 (1999) 247-257. https://doi.org/210.1016/S0926-3373(1099)00082-X.
[68] C. Thomas, O. Gorce, C. Fontaine, J.-M. Krafft, F. Villain, G. Djéga-Mariadassou, On the promotional effect of Pd on the propene-assisted decomposition of NO on chlorinated $Ce_{0.68}Zr_{0.32}O_2$, Appl. Catal. B: Environmental, 63 (2006) 201-214. https://doi.org/210.1016/j.apcatb.2005.1009.1010.
[69] M. Ogura, R. Guillet-Nicolas, D. Brouri, S. Casale, J. Blanchard, K.A. Cychosz, M. Thommes, C. Thomas, Insights into the accessibility of Zr in Zr/SBA-15 mesoporous silica supports with increasing Zr loadings, Microporous Mesoporous Mater., 225 (2016) 440-449. https://doi.org/410.1016/j.micromeso.2016.1001.1026.
[70] W.-X. Zhang, H. Yahiro, M. Iwamoto, J. Izumi, Reversible and irreversible adsorption of nitrogen monoxide on cobalt ion-exchanged ZSM-5 and mordenite zeolites at 273–523 K, J. Chem. Soc. Faraday Trans., 91 (1995) 767-771. https://doi.org/710.1039/FT9959100767.
[71] L. Čapek, J. Dědeček, P. Sazama, B. Wichterlová, The decisive role of the distribution of Al in the framework of beta zeolites on the structure and activity of Co ion species in propane–SCR–NO_x in the presence of water vapour, J. Catal., 272 (2010) 44-54. https://doi.org/10.1016/j.jcat.2010.1003.1013.
[72] Z. Bian, N. Dewangan, Z. Wang, S. Pati, S. Xi, A. Borgna, H. Kus, S. Kawi, Mesoporous-silica-stabilized cobalt (II) oxide nanoclusters for propane dehydrogenation, ACS Appl. Nano Mater., 4 (2021) 1112-1125. https://dx.doi.org/1110.1021/acsanm.1110c02721.
[73] J. Xie, J.D. Kammert, N. Kaylor, J.W. Zheng, E. Choi, H.N. Pham, X. Sang, E. Stavitski, K. Attenkofer, R.R. Unocic, Atomically dispersed Co and Cu on N-doped carbon for reactions involving C–H activation, ACS Catal., 8 (2018) 3875-3884. https://doi.org/3810.1021/acscatal.3878b00141.
[74] W. Wang, Y. Wu, T. Liu, Y. Zhao, Y. Qu, R. Yang, Z. Xue, Z. Wang, F. Zhou, J. Long, Single Co sites in ordered SiO_2 channels for boosting nonoxidative propane dehydrogenation, ACS Catal., 12 (2022) 2632-2638. https://doi.org/2610.1021/acscatal.2631c05921.
[75] B. Wollak, D. Doronkin, D. Espinoza, T. Sheppard, O. Korup, M. Schmidt, S. Alizadefanaloo, F. Rosowski, C. Schroer, J.-D. Grunwaldt, R. Horn, Exploring catalyst dynamics in a fixed bed reactor by correlative operando spatially-resolved structure-activity profiling, J. Catal., 408 (2022) 372-387. https://doi.org/310.1016/j.jcat.2021.1008.1029.
[76] S. Petit, C. Thomas, Y. Millot, J.M. Krafft, C. Laberty-Robert, G. Costentin, Activation of C–H Bond of propane by strong basic sites generated by bulk proton conduction on V-modified hydroxyapatites for the formation of propene, ChemCatChem, 12 (2020) 2506-2521. https://doi.org/2510.1002/cctc.201902181.
[77] B. Solsona, T.E. Davies, T. Garcia, I. Vázquez, A. Dejoz, S.H. Taylor, Total oxidation of propane using nanocrystalline cobalt oxide and supported cobalt oxide catalysts, App. Catal. B: Environmental, 84 (2008) 176-184. https://doi.org/110.1016/j.apcatb.2008.1003.1021.
[78] R. Baran, Y. Millot, F. Averseng, S. Dzwigaj, Vanadium incorporation from aqueous NH_4VO_3 solution into siliceous Beta zeolite determined by NMR with formation of V-single site zeolite catalysts for application in SCR of NO, Appl. Catal. A: General, 606 (2020) 117830. https://doi.org/117810.111016/j.apcata.112020.117830.

Supporting Information

Cobalt on Dealuminated-Siβ as a Catalyst for the Oxidative Dehydrogenation of Propane

Stanislaw Dzwigaj, Diane Reja, Saremblé Koné-Guira, Antoine Miche,

Guylène Costentin and Cyril Thomas*

Sorbonne Université, CNRS, Laboratoire Réactivité de Surface, LRS, F-75005 Paris, France.

* To whom correspondence should be addressed:

Dr. Cyril Thomas

Sorbonne Université, CNRS, Laboratoire Réactivité de Surface, LRS, UMR CNRS 7197, 4 Place Jussieu, Tour 43-53, 3ème étage, Case 178, F-75252, Paris, France

e-mail: cyril.thomas@sorbonne-universite.fr

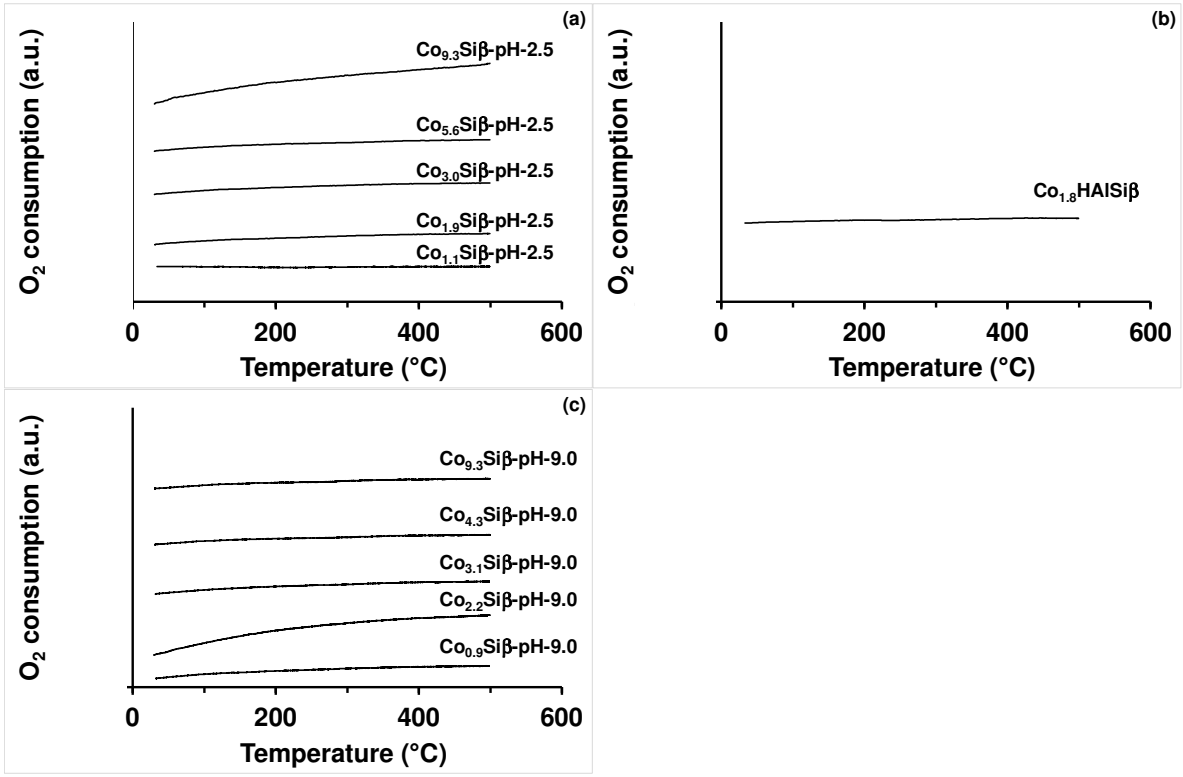

Figure S1. O_2-TPO profiles recorded from RT to 500 °C in 5% O_2/He with a 25 mL/min flow rate and a heating rate of 10 °C/min on (a) Co_x-Siβ-pH-2.5, (b) $Co_{1.8}$-HAlSiβ and (c) Co_x-Siβ-pH-9.0.

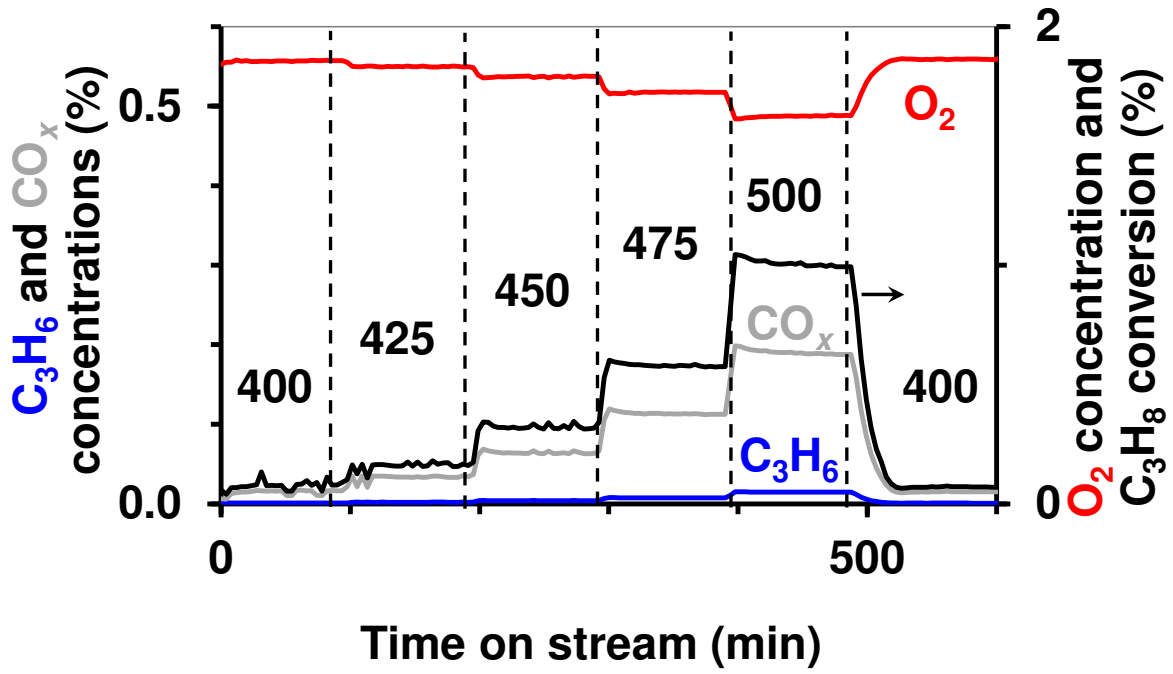

Figure S2. Evolution of the conversion of C_3H_8 (black trace) and the concentrations in C_3H_6 (blue trace), O_2 (red trace) and CO_x (gray trace) (8.2% C_3H_8, 1.9% O_2 in He, 74.1 mL_{NTP} min^{-1} total flow) as a function of time on stream and reacting temperature on 600 mg of α-Al_2O_3. The numbers reported on the figure are related to the reaction temperature.

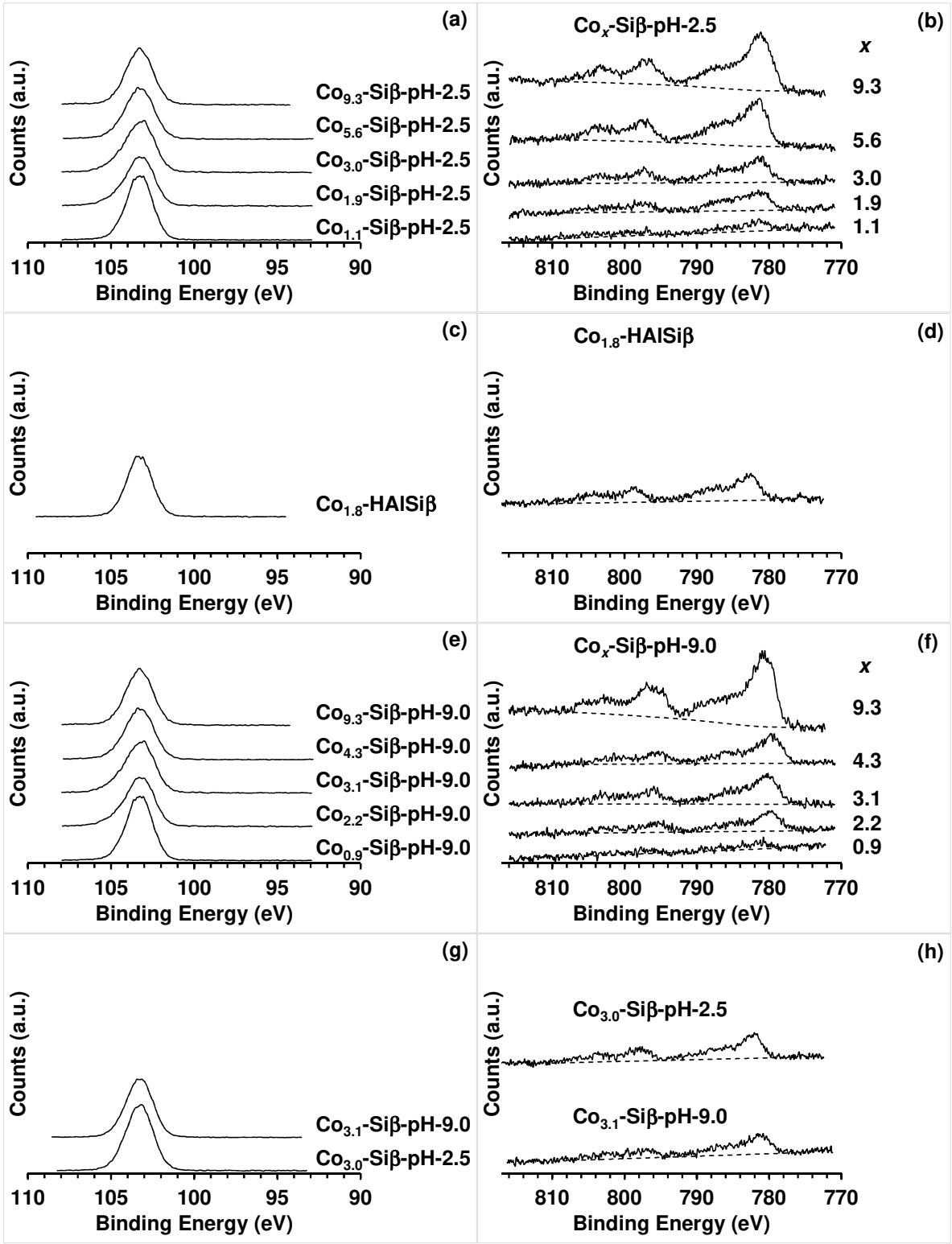

Figure S3. Si 2p (a, c, e, g) and Co 2p (b, d, f, h) core levels of the various samples before (a-f) and after (g,h) ODHP reaction.

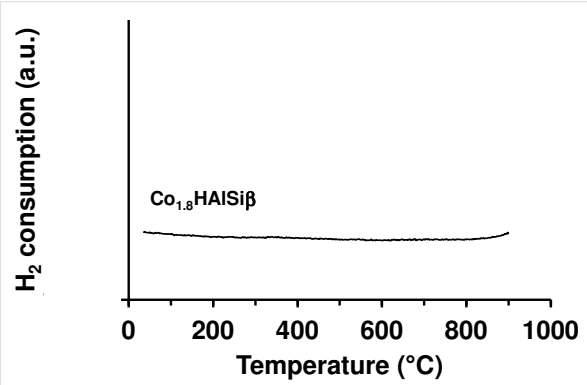

Figure S4. H_2-TPR profile recorded from RT to 900 °C in 5% H_2/Ar with a 25 mL/min flow rate and a heating rate of 10 °C/min on $Co_{1.8}$-HAlSiβ calcined at 500 °C (10 °C/min) under 5%O_2/He for 1 h.

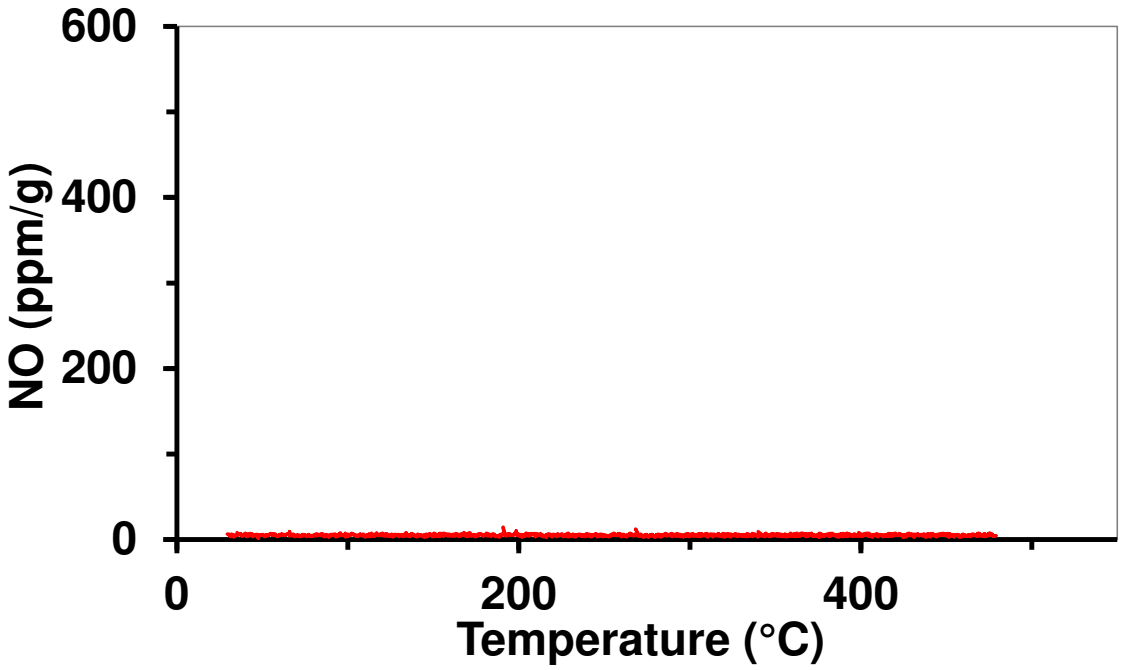

Figure S5. NO-TPD profile recorded on 120 mg of Siβ after annealing of the sample at 500 °C for 2 h in 100 mL_{NTP} min^{-1} of He and RT exposure to 230 mL_{NTP} min^{-1} of NO(400 ppm) in He for 2 h followed by temperature-programmed desorption from RT to 500 °C (3 °C min^{-1}) in 230 mL_{NTP} min^{-1} of He.

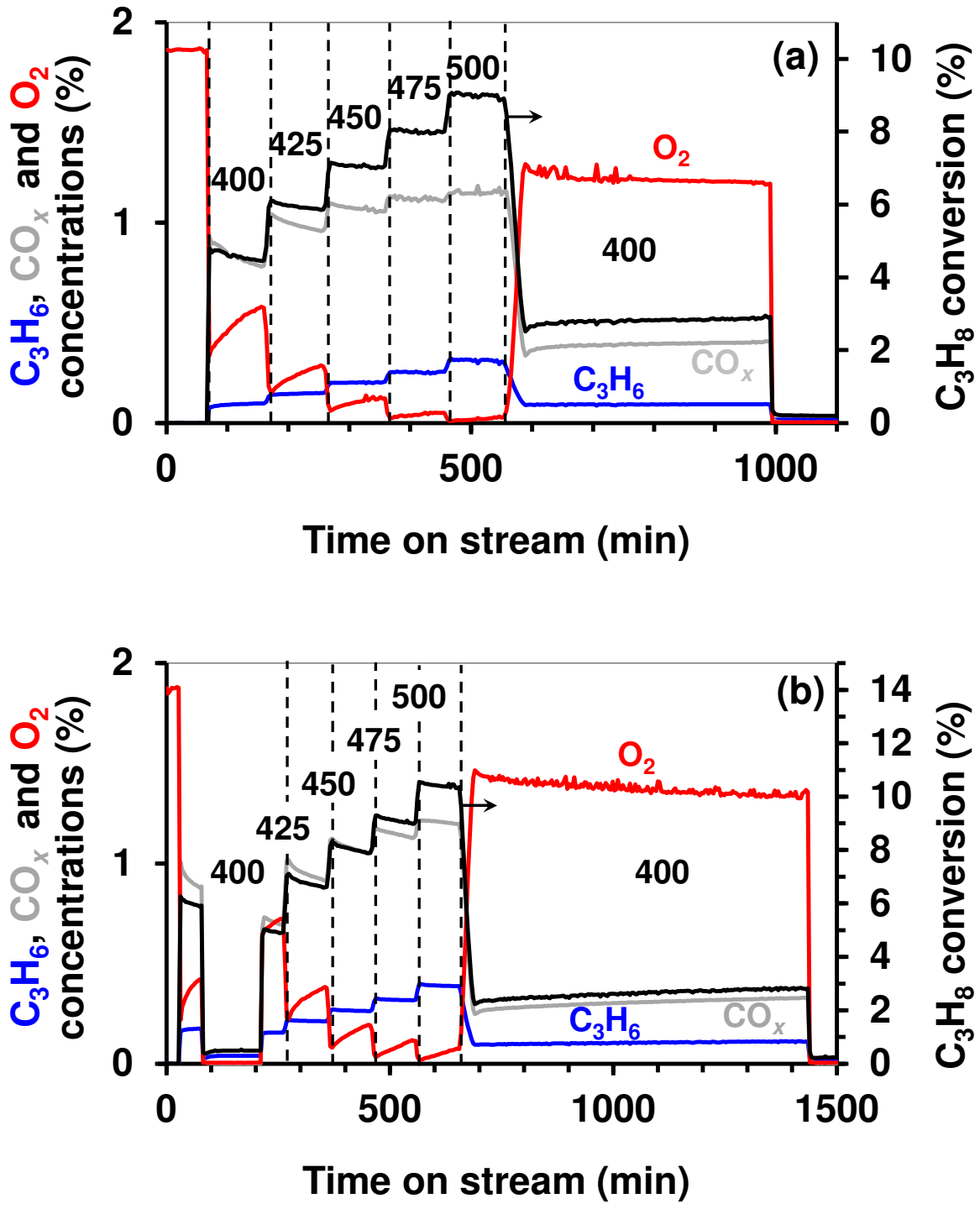

Figure S6. Influence of the removal of O_2 from a 8.2% C_3H_8 (8.2%) – O_2 (1.9%) – He feed at 400 °C after ODHP reaction from 400 to 500 °C on (a) $Co_{3.0}$-Siβ-pH-2.5 and (b) $Co_{3.1}$-Siβ-pH-

9.0 on the propane conversion (black trace) and CO_x (gray trace), C_3H_6 (blue trace) and O_2 (red trace) concentrations.

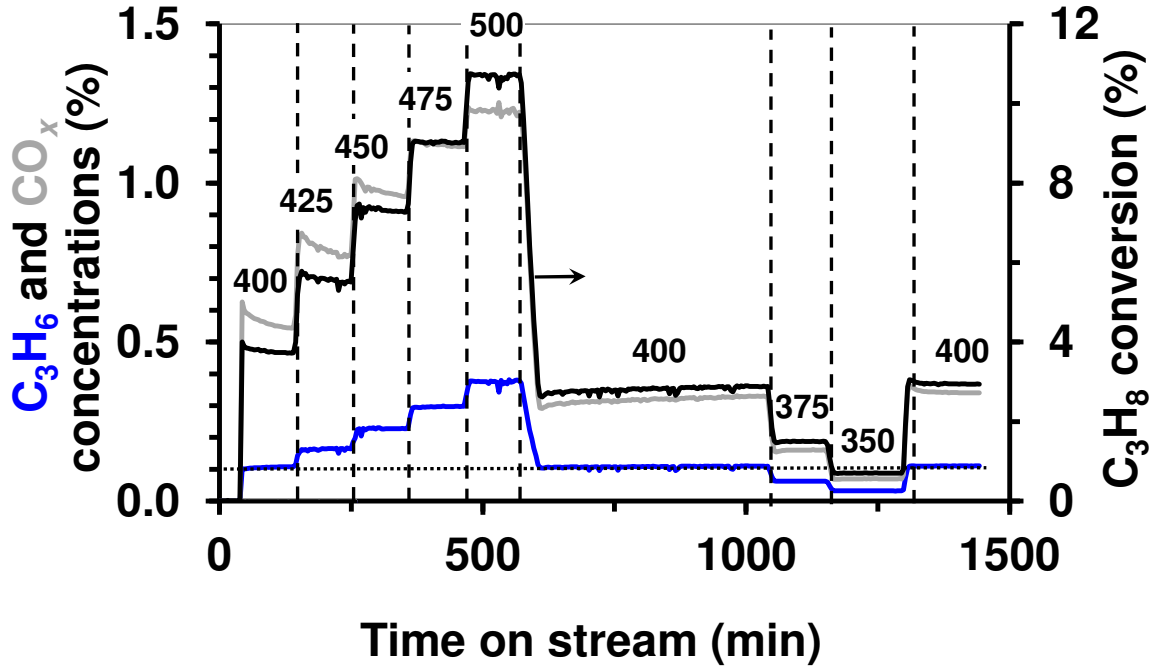

Figure S7. Evolution of the conversion of C_3H_8 (black trace) and the concentrations in C_3H_6 (blue trace) and CO_x (gray trace) (8.2% C_3H_8, 1.9% O_2 in He, 74.1 mL_{NTP} min^{-1} total flow) as a function of time on stream and reacting temperature on 60 mg of $Co_{1.9}$-Siβ-pH-2.5 diluted in 600 mg of α-Al_2O_3. The numbers reported on the figures are related to the reaction temperature.

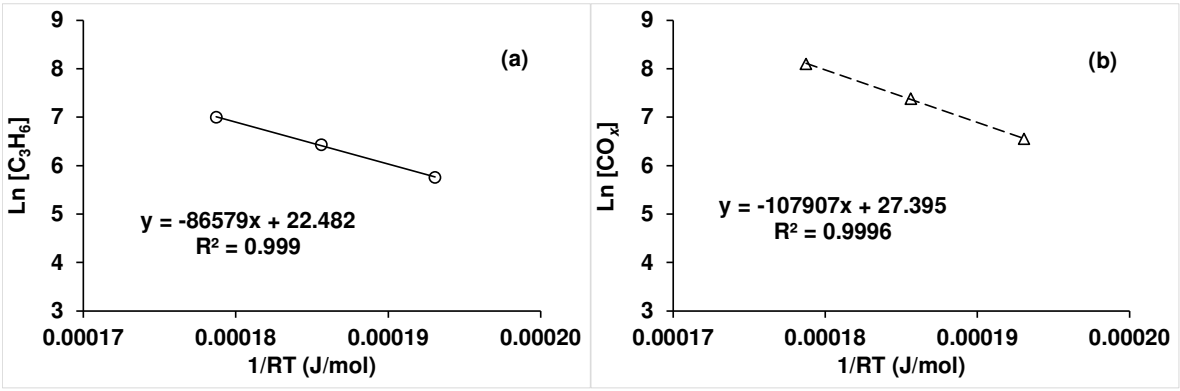

Figure S8. Arrhenius plots for the formation of (a) C_3H_6 and (b) CO_x over 60 mg of $Co_{1.9}$-Siβ-pH-2.5 diluted in 600 mg of α-Al_2O_3 in the 350-400 °C temperature range (8.2% C_3H_8, 1.9% O_2 in He, 74.1 mL_{NTP} min^{-1} total flow).